Materials Today Bio 27 (2024) 101151

Contents lists available at ScienceDirect

Materials Today Bio

journal homepage: www.journals.elsevier.com/materials-today-bio

Contribution of Tregs to the promotion of constructive remodeling after decellularized extracellular matrix material implantation

Hongjing Jiang [a,b], Xuheng Sun [a], Yindi Wu [a,b], Jianyi Xu [a], Cong Xiao [a], Qing Liu [a], Lijun Fang [a], Yuanfeng Liang [c], Jiahui Zhou [b], Yueheng Wu [b,d], Zhanyi Lin [a,b,d,*]

[a] School of Medicine, South China University of Technology, 510006, Guangzhou, Guangdong, China
[b] Guangdong Provincial People's Hospital (Guangdong Academy of Medical Sciences), Southern Medical University, 510080, Guangzhou, Guangdong, China
[c] Department of Geriatrics, Guangdong Provincial Geriatrics Institute, Guangdong Provincial People's Hospital (Guangdong Academy of Medical Sciences), Southern Medical University, 510006, Guangzhou, Guangdong, China
[d] Ji Hua Institute of Biomedical Engineering Technology, Ji Hua Laboratory, 528200, Foshan, Guangdong, China

ARTICLE INFO

Keywords:
Tregs
Decellularization
ECM
Remodeling
Macrophages

ABSTRACT

Host remodeling of decellularized extracellular matrix (dECM) material through the appropriate involvement of immune cells is essential for achieving functional organ/tissue regeneration. As many studies have focused on the role of macrophages, only few have evaluated the role of regulatory T cells (Tregs) in dECM remodeling. In this study, we used a mouse model of traumatic muscle injury to determine the role of Tregs in the constructive remodeling of vascular-derived dECM. According to the results, a certain number of Tregs could be recruited after dECM implantation. Notably, using anti-CD25 to reduce the number of Tregs recruited by the dECM was significantly detrimental to material remodeling based on a significant reduction in the number of M2 macrophages. In addition, collagen and elastic fibers, which maintain the integrity and mechanical properties of the material, rapidly degraded during the early stages of implantation. In contrast, the use of CD28-SA antibodies to increase the number of Tregs recruited by dECM promoted constructive remodeling, resulting in a decreased inflammatory response at the material edge, thinning of the surrounding fibrous connective tissue, uniform infiltration of host cells, and significantly improved tissue remodeling scores. The number of M2 macrophages increased whereas that of M1 macrophages decreased. Moreover, Treg-conditioned medium further enhanced material-induced M2 macrophage polarization *in vitro*. Overall, Treg is an important cell type that influences constructive remodeling of the dECM. Such findings contribute to the design of next-generation biomaterials to optimize the remodeling and regeneration of dECM materials.

1. Introduction

Decellularized extracellular matrix (dECM) scaffolds are ideal for regenerating functional organs and tissues. Decellularization removes cell-associated antigens and creates a dECM that retains its ultrastructure and composition. The dECM scaffold is mainly composed of an extracellular matrix (ECM), which is a three-dimensional (3D) framework containing collagen, elastin, fibronectin, and laminin [1]. The dECM provides a substrate for mechanical support and a matrix carrier for subsequent cell growth. Notably, dECM material is used in many tissue types, including cartilage, fat, muscle, skin, lung, and blood vessels. However, one of the greatest challenges faced by this class of decellularized grafts, especially vascular grafts, is their ability to be adopted and remodeled into new tissues by the host [2].

Based on increasing evidence, immune cells play a critical role in remodeling. Immune cells arrive at the biomaterial site early after implantation. By secreting cytokines, immune cells establish a microenvironment for subsequent cell infiltration, proliferation, and differentiation or even participate directly in the regeneration process [3]. Previous studies have focused on the role of macrophages in dECM remodeling. Based on current consensus, macrophages play an important role in tissue regeneration and remodeling [4]. The host immune response to an implanted biomaterial, particularly the phenotype of infiltrating macrophages, is a key determinant of downstream remodeling [5,6]. In particular, persistent pro-inflammatory M1 macrophages are associated with less favorable outcomes and are characterized by

* Corresponding author. School of Medicine, South China University of Technology, 510006, Guangzhou, Guangdong, China.
E-mail address: linzhanyi@gdph.org.cn (Z. Lin).

https://doi.org/10.1016/j.mtbio.2024.101151
Received 15 April 2024; Received in revised form 2 July 2024; Accepted 7 July 2024
Available online 9 July 2024

dense fibrosis, scar tissue, and chronic inflammation [7,8]. However, at the early stages of graft implantation, M1 macrophages are essential for initiating responses involved in the downstream promotion of regeneration and resolution [9,10]. Over time, the rapid transition of infiltrating macrophages from an initial M1 response to an M2 phenotype is associated with a constructive remodeling response characterized by the resolution of inflammation and deposition of more organized, site-appropriate tissues [11,12].

Although macrophages and their various polarized states have been identified as important mediators of dECM remodeling [11], recent evidence suggests that the adaptive immune system is a key factor. Th2 cells help coordinate healing and functional tissue repair after muscle loss and implantation of biological ECM scaffolds. These cells promote Interleukin 4 (IL4) expression at the wound site and the M2 macrophage phenotype. Regulatory T cells (Tregs) are also present at the wound site, and their numbers increase over time [13]. Tregs play crucial roles in immune homeostasis and have been described to modulate immunity during transplant rejection [14]. Uncontrolled inflammation can lead to impaired tissue remodeling. However, Tregs can suppress overactive and regulate uncontrolled inflammation to facilitate immune system homeostasis [15,16]. In many tissues, Tregs are recruited to damaged sites to facilitate inflammation resolution and regulate immunity after injury [17]. Studies have shown that Tregs are central to the repair and regeneration of several tissues, including the skin [18], bone [19,20], lungs [21], kidney [22], skeletal muscle [23], and cardiac muscle [24]. The presence of Tregs results in the production of arginase and anti-inflammatory cytokines, such as IL10 and TGF-β. These secreted factors provide an anti-inflammatory microenvironment that can control neutrophils [25–27], regulate helper T-cells [27,28], and promote macrophage polarization to the M2 phenotype [27,29–32]. Moreover, Tregs can directly facilitate tissue regeneration by activating tissue-specific stem and progenitor cells [18,33–35]. Biomaterial implantation creates a unique immune microenvironment. After dECM implantation, the role of Tregs in the immune microenvironment during material remodeling has not been reported. Owing to the ability of Tregs to modulate inflammation, we hypothesized that Tregs influence dECM material remodeling. Understanding the immune response to dECM will aid in the efficient design of immune engineering strategies to optimize the remodeling and regeneration of decellularized materials.

In this study, we selected a dECM material derived from the bovine aorta. This material was selected because dECM vascular material is a promising source of grafts. All vascular xenografts, allografts, and some tissue-engineered vascular grafts, such as human acellular vessels (HAVs), as described by Niklason [15], are decellularized. However, arterial-derived dECM is structurally denser than other dECMs. Dense-matrix tissues can limit cell migration to the scaffold material, compromising the proper proliferation of host cells, thereby affecting host remodeling into its own living tissue [36,37]. Therefore, the role of Tregs in the remodeling of dense dECM materials must be investigated. Different approaches have been used to determine the contribution of Tregs. First, by inducing an anti-CD25 monoclonal antibody-mediated reduction in Treg numbers, we found that reduced Treg recruitment to the dECM led to the rapid degradation of collagen and elastic fibers. However, collagen and elastic fibers can maintain the mechanical properties and matrix integrity of the dECM. In contrast, the expansion of Tregs by superagonistic CD28-specific monoclonal antibodies (CD28-SA) and the increased recruitment of Tregs by dECM significantly promoted constructive remodeling. Polarization of macrophages to M2 is essential for biomaterial remodeling. Therefore, we focused specifically on the Treg-mediated regulation of macrophage polarization. The results of the *in vitro* and *in vivo* experiments indicate that Tregs can promote the polarization of macrophages to M2 in the immune microenvironment of dECM. These findings suggest the important role of Tregs in dECM remodeling, which is critical for guiding future design of immune cells to establish a pro-remodeling microenvironment.

2. Materials and methods

2.1. Preparation of the dECM material

The animal experimental protocols were approved by the Ethics Review Committee of Guangdong Provincial People's Hospital (approval ID: KY2023-192-01). Adult bovine aortas were procured from the closest abattoir and subjected to a standard protocol. The tissues were cleaned with distilled water to remove all traces of blood. Subsequently, the tissues were washed thrice with PBS (Sigma Aldrich, USA). Decellularization was performed as previously described [15]. The native aorta was subjected to a 24-h rinse in a mixture of zwitterionic detergent (8 mM CHAPS) and anionic detergent (1.8 mM SDS). The tissues were washed with PBS until all air bubbles were cleared. Following rinsing with PBS, the tissues were transferred to a solution composed of PBS and 10 % fetal bovine serum (FBS, Corning, USA) and rinsed for 24 h. All procedures were conducted at 37 °C with 5 % CO_2. Post-decellularization, all dECM underwent a PBS rinse. Samples were stored in sterile PBS at 4 °C prior to use.

2.2. DNA quantification and qualitative fragment analysis

The native and dECM materials were placed in a freeze-dryer, and the scaffolds were lyophilized under constant vacuum. Thereafter, the samples were digested overnight in a papain solution (125 μg/mL papain, 5 mmol/L cysteine acid, and 5 mmol/L ethylene diamine tetraacetic acid). DNA concentration was quantified using the PicoGreen dsDNA Quantitation Assay Kit (PicoGreen®, Invitrogen, USA), according to the manufacturer's instructions. The fluorescence of the plate was measured using a Synergy 2 microplate reader (BioTek, USA) at excitation and emission wavelengths of 480 and 520 nm, respectively. For qualitative fragment length analysis, total DNA was separated electrophoretically on a 1.5 % agarose gel for 50 min at 120 V. The results were documented using a gel imaging system (Tanon, China).

2.3. Scanning electron microscopy

Native and dECM samples were prepared for SEM analysis via overnight fixation in 2.5 % glutaraldehyde solution, followed by dehydration using a series of ethanol solutions. The samples were air-dried, positioned on aluminum stubs, and sputter-coated with gold (Leica, Germany). Imaging was performed using Verios 5 UC SEM (Thermo Fisher Scientific, USA).

2.4. Mechanical properties

Native and dECM samples were cut into 3 cm × 3 cm strips. The thicknesses of five random points on the strip were measured using a thickness gauge. Thereafter, the average thickness (H) was determined. Each side of the strip was attached to the clamp of a biaxial tensile tester (BioTester, CellScale, Canada). The initial distance between the two clamps was denoted as L0. The strip was stretched at 6 mm/min until failure and the force (F) and distance between the two clamps (L) were recorded. Subsequently, a stress-strain plot of the sample was obtained. Young's modulus of the tissue was determined by dividing the stress by the strain.

Determination of suture strength: One end of the native and dECM samples was fixed, and the other end was punctured with a 6-0 prolene suture 3 mm from the edge. Weights were sequentially added to record the weight at the time of failure.

2.5. Hydrophilic properties

The hydrophilicity of the native and dECM samples was measured using a dynamic contact angle meter (Dataphysics, Germany). Deionized water (5 μL) was dispensed at three different locations on the material

surface and then the contact angle values was detected under ambient conditions.

2.6. Cytotoxicity

Direct contact experiment: The dECM was fixed at the center of a six-well culture plate using a CELL-TISSUE (Corning, USA). Sterile gauze containing 10 % SDS (m/v) and plain sterile gauze were used as the positive and negative controls, respectively. Human fibroblasts (5×10^5 cells/mL, CTCC-180-HUM, Meisen CTCC, China) were inoculated into each well and 2 mL of DMEM (Gibco, USA) containing 10 % FBS (Corning, USA) was added to each well. The culture plate was incubated at 37 °C in 5 % CO_2 for 48 h and then observed under a microscope. Trypsin (0.25 %, Gibco, USA) was used to digest adherent cells, and the cell suspension was collected, mixed with 0.4 % trypan blue (1:1, Macklin, China), and stained for 5 min. Dead and living cells were counted using a cell counter.

For indirect contact experiments, the dECM material was placed in complete medium at a ratio of per square centimeter/2.5 mL. The extract was prepared for 24 h at 37 °C in a 5 % CO_2 incubator. A complete medium without dECM under the same conditions was used as the control medium. The extracts were diluted with fresh complete medium at ratios of ½, ¼, and $^1/_8$. The CCK-8 assay (Dojindo, Kumamoto, Japan) was conducted to determine the effects of different extract proportions and control media on the viability of human fibroblasts after 24 h of culture. Following the manufacturer's instructions, the CCK-8 reagent was added at the end of the incubation period and the sample was incubated for 2 h before the absorbance was measured at 450 nm. Human fibroblasts were cultured for 48 h after mixing the extract/control medium 1:1 with the complete medium. The extract served as the dECM group, and the control medium served as the control group. Cell viability was assessed using a Live/Dead Cell Assay Kit (Beyotime). Live and dead cells were imaged using a fluorescence microscope (Olympus, Tokyo, Japan). Cell viability was calculated using the following formula: cell viability (%) = (number of calcein-AM^+ cells)/(number of calcein-AM^+ cells + number of PI^+ cells) × 100. Phalloidin staining (Proteintech, USA) was used to detect cytoskeletal changes. Cells were fixed with 4 % PFA, according to the manufacturer's instructions, permeabilized with 0.2 % Triton X-100 at room temperature, and treated with a phalloidin solution. Phalloidin-stained images were captured using an LSM980 confocal microscope (Carl Zeiss, Germany). The length and width of 80 cells per group were measured using ImageJ software. The cell length was divided by the width to obtain the length-to-width ratio.

2.7. Mouse surgical procedures

All animals were purchased from Guangdong Medical Laboratory Animal Center (Laboratory Animal Production License No. SCXK 2022-0002). Eight-week-old SPF C57BL/6 mice were used to establish the implantation models. All mouse experiments were performed using protocols approved by the Ethics Review Committee of Guangdong Provincial People's Hospital (approval ID: KY2023-201-01). All animals were housed under specific pathogen-free conditions (24 °C, 12-h light/12-h dark cycles, and 50 % humidity) with free access to food pellets and tap water. The animals were handled in accordance with the Guide for the Care and Use of Laboratory Animals.

The dECM, with a size of 0.3 cm length, 0.3 cm width, and 0.1 cm height, was prepared before implantation. Implantation was performed as previously described [13]. Briefly, after mice were anesthetized via an intraperitoneal injection of pentobarbital sodium (45 mg/kg), their lower limb hair was removed with an electric razor. After ethanol sterilization of the surrounding skin, a 1.2-cm incision was made between the knee and hip joints to access the quadriceps femoris muscle. Surgical scissors were used to create a traumatic wound, and dECM was implanted in the quadriceps femoris muscle of mice. The skin was closed using absorbable 5-0 suture. The animals recovered from anesthesia on a heating pad and were allowed to carry out normal activity while the right leg was used as the dECM group (dECM material was implanted). Animals in the sham group underwent the same surgical procedure but received no implants. After follow-ups on days 3, 7, 14, or 28 (n = 5 at each time point), the animals were anesthetized and killed, and their entire quadriceps femoris muscle (cut from the knee joint along the femur to the hip joint) and dECM material were explanted for further investigation. Subsequently, the dECM was immersed in a 4 % PFA solution and embedded in paraffin.

To reduce the recruitment of Tregs, mice were intraperitoneally injected with 250 μg of anti-CD25 monoclonal antibody (clone PC61, 102040, Biolegend, USA) one day before implantation and 7 days after implantation (n = 5). To increase the recruitment of Tregs, mice were intraperitoneally injected with 200 μg of superagonistic anti-CD28 monoclonal antibody (CD28-SA, clone D665, BE0328, BioXcell, USA) on the day before implantation and 7 days after implantation (n = 5). Mice in the control group were injected with an isotype control antibody (BioLegend, USA) at the same time and dose (n = 5). The left and right legs of anti-CD25, CD28-SA, and control mice were implanted with dECM. On day 14 after implantation, mice were anesthetized and killed, and their entire quadriceps femoris muscle and dECM were harvested for detection.

2.8. Histology and immunofluorescence

For histological analysis, the dECM material was fixed in 4 % PFA for 24 h and progressively dehydrated using low-to-high gradient concentrations of alcohol. The tissue was immersed in wax and then cut into slices with a thickness of 5 μm. The sections were stained with hematoxylin and eosin (HE), EVG, Masson's, and Sirius red to observe the general morphology, cell infiltration, and expression of elastic and collagen fibers, respectively. The slices were scanned using NanoZoomerS360 (Hamamatsu Photonics, Japan). Sirius red-stained slides were scanned and imaged using a SLIDEVIEW VS200 microscope (Olympus, Japan) under a polarized light field. In the EVG, Masson, and Sirius Red stained images, the percentage of the area covered by the positive signal in the total area of the image was used as the quantitative signal data. Image-Pro Plus 6.0 (USA) was used for the calculations. Histological sections were scored blindly by two experienced histopathologists on day 14 using scoring criteria previously validated for the response to inflammation and tissue remodeling [11].

For immunofluorescence, the paraffin sections were dewaxed in water and the antigens were repaired at high temperature and pressure. To assess Treg infiltration into the dECM material, the sections were sealed with 10 % donkey serum (AntGene, China), and then incubated with forkhead box protein P3 (Foxp3) (1:200, 12653, CST, USA) antibody working fluid. The next day, the section was incubated with the second antibody, Alexa Fluor®594 donkey anti-rabbit lgG (H + L) (1:600, A21207, Life Technologies, USA). Finally, DAPI (C0060, Solarbio, China) staining was performed, and the film was sealed for microscopy. $Foxp3^+$ $DAPI^+$ cells were counted in each section and the dECM material area was calculated. Data are presented as the ratio of $Foxp3^+$ $DAPI^+$ cells to the dECM material area. For macrophage staining, the pan-macrophage marker F4/80 and phenotypic markers for M1 CD86 and M2 CD206 macrophages were used to assess the macrophage responses. Briefly, antigen repair was performed after paraffin sections were deparaffinized in water. Sections were blocked via incubation with 3 % H_2O_2 for 30 min at room temperature. After blocking with 10 % goat serum (Boster, China) at room temperature for 30 min, the sections were incubated overnight with CD86 antibody (1:400, 19589, CST, USA) working solution at 4 °C. The following day, the sections were incubated with a working solution of horseradish peroxidase (HRP)-conjugated secondary goat anti-rabbit IgG antibody (1:4000, ab205718, Abcam, UK) at 37 °C for 45 min. After washing with TBST, the sections were incubated with CY5 (1:400, 11066, Aatbio, USA) working solution at

room temperature for 10 min. After additional TBST washes, antigen repair was performed, and then the sections were incubated with 10 % goat serum for 30 min at room temperature. After blocking, the sections were incubated overnight with the F4/80 antibody (1:1000, 70076, CST, USA) working solution at 4 °C, followed by goat anti-rabbit IgG:HRP working solution at 37 °C for 45 min. After washing with TBST, the sections were incubated with FITC (1:300, 11060, Aatbio, USA) working solution at room temperature for 10 min. The antigen repair and blocking steps were repeated and then the sections were incubated overnight with the CD206 antibody (1:1000, 24595, CST, USA) working solution at 4 °C. At the end of the incubation period, the sections were incubated with goat anti-rabbit IgG:HRP secondary antibody working solution at 37 °C for 45 min. After washing with TBST, the sections were incubated with CY3 (1:600, 11065, Aatbio, USA) working solution at room temperature for 10 min. Finally, DAPI working solution was added dropwise, and the slides were sealed for microscopic examination. The entire dECM material was scanned using a 3DHistech (Pannoramic MIDI, Hungary). $DAPI^+$, $F4/80^+$ $DAPI^+$, $F4/80^+$ $CD206^+$ $DAPI^+$, and $F4/80^+$ $CD86^+$ $DAPI^+$ cells were counted in the entire dECM material. The data are expressed as the proportion of positive cells.

2.9. Flow cytometry of dECM-associated immune cells

Muscle wounds and dECM surrounding area were harvested by cutting the quadriceps muscle from the hip to the knee and finely diced in PBS on ice, digested for 45 min at 37 °C in an enzyme solution consisting of 1.67 Wunsch U/mL Liberase TL (5401020001, Roche, Switzerland) and 0.2 mg/mL benzonase (E1014, Merck Millipore, Germany) in RPMI 1640, and filtered through 70 μm cell strainers. The cells were then washed twice with PBS, suspended in 40 % Percoll (Sigma Aldrich, USA), and layered over 80 % Percoll for density centrifugation at 500×*g* for 30 min. Enriched cells were collected during interphase. The collected cells were washed twice with PBS and resuspended in PBS for further analyses.

The cells were stained on ice using the Zombie NIR™ Fixable Viability Kit (1:500, 423105, Biolegend, USA), followed by a cocktail of surface markers. The Treg panel included antibodies against CD45 Brilliant Violet 510 (103137, BioLegend), CD3 PE/CY7 (100219, BioLegend), CD4 FITC (11-0041-82, eBioscience), CD25 APC (17-0251-81, eBioscience), and Foxp3 (12-4774-41, eBioscience). The macrophage panel included CD45 Brilliant Violet 510 (103137, BioLegend), F4/80 (123107, BioLegend), CD11 b PE/Cyanine7 (101215, BioLegend), CD206 APC (141707, BioLegend), and CD86 PE (159203, BioLegend). For intracellular staining, the cells were first stained using surface markers, and then fixed and permeabilized using the Foxp3 Transcription Factor Staining Buffer Set (00-5523-00, eBioscience, USA), according to the manufacturer's instructions, followed by intracellular staining. All antibodies were used at the recommended concentrations. The data were collected using a CytoFLEX Flow Cytometer (Beckman Coulter, USA) and analyzed using the FlowJo software (version 10.8.1, TreeStar, USA).

2.10. Determination of collagen and elastin content in the dECM material

A hydroxyproline (HYP) content detection kit (BC0255, Solarbio, China) was used to determine the collagen content, according to the manufacturer's instructions. Briefly, the dECM material from the control and anti-CD25 groups was digested at 100 °C with 6 M hydrochloric acid after weighing. The pH value was then adjusted to the range of 6–8 using 10 M NaOH. After a constant volume was achieved, the samples were centrifuged at 16000 rpm for 20 min at 25 °C and the supernatant was collected. Following incubation with the reagent provided in the kit, the absorbance was measured at 560 nm. The tissue hydroxyproline content was calculated according to the formula provided by the kit and normalized to that of the control.

The Fastin Elastin Assay (F2000, Biocolor, UK) was used to determine the elastin content, according to the manufacturer's instructions. Briefly, after weighing of the dECM material from the control and anti-CD25 groups, 0.25 M oxalic acid was added, and the samples were incubated at 100 °C for 60 min to convert insoluble elastin into water-soluble α-elastin. An equal volume of the elastin-precipitating reagent was then added, and the pellet was collected after centrifugation at 13000×*g* for 10 min. One mL of the Dye Reagent was added, and the samples were incubated on a shaker for 90 min. After centrifugation at 13000×*g* for 10 min, the pellet was collected, resuspended in 250 μL of Dye Dissociation Reagent, and mixed to a homogenous solution before measuring the absorbance at 513 nm. The elastin content of the samples was calculated and normalized to that of the control group using an elastin standard curve.

2.11. RNA sequencing

$F4/80^+$ macrophages were enriched from control and CD28-SA dECM using the EasySep mice F4/80 Pos Sel Kit (100–0659, StemCell, Canada). For RNA extraction and library construction, total RNA was isolated and purified using TRIzol reagent (Invitrogen, USA). RNA integrity was assessed using a Bioanalyzer 2100 (Agilent Technologies). The SMART method was used for pre-amplification of samples and library construction. Illumina Novaseq™ 6000 was used to sequence the library after qualified quality inspection. Hisat software was used to compare the sequencing data with the reference genome, and StringTie software was used to assemble the transcripts and calculate their expression levels. Subsequently, edgeR was used for differential expression analysis, and R software was used to graphically display the differential expression results, including differentially expressed gene heat maps as well as volcano and principal component analysis maps. Additional functional analysis of the differentially expressed genes was performed using Gene Ontology (GO) and Kyoto Encyclopedia of Genes and Genomes (KEGG) pathway enrichment.

2.12. Preparation of solubilized dECM material

As previously mentioned [38], the prepared dECM material was freeze-dried and ground into a powder. An ECM solution containing 10 mg/mL of dECM was dissolved in pepsin (Sigma Aldrich, USA). The ECM solution was then neutralized by adding 1/10 volume of NaOH (0.1 N) and 1/9 volume of 10 × PBS; thus, the pH was 7.4.

2.13. Preparation of Treg-conditioned medium

Tregs were isolated from eight-week-old SPF C57BL/6 mouse spleens using the EasySep Mouse CD25 Treg Pos Sel Kit (18782, StemCell, Canada). Culture plates were coated with CD3 antibodies (10 μg/mL, 100339, BioLegend, USA), and Tregs were cultured in RPMI 1640 medium (Hyclone, USA) supplemented with CD28 (1 μg/mL, 102115, BioLegend, USA), IL2 (30 ng/mL, PEPROTECH, USA), and 10 % FBS. After three days of culture, CD3 and CD28 were removed, and Tregs were cultured with IL-2 (30 ng/mL, PEPROTECH, USA) and 10 % FBS. The cell medium was collected and centrifuged at 3000 rpm for 10 min. Finally, the supernatant was collected, filtered through a 0.22 μm membrane, and stored at −80 °C.

2.14. Polarization of bone marrow-derived macrophages (BMDMs)

After sterile separation of the femur and tibia from eight-week-old SPF C57BL/6 mice, the bone was cut from both ends and washed with RPMI 1640 medium to collect the bone marrow. The bone marrow was washed thrice until the bone marrow cavity turned white. After the cell suspension was passed through a 70 μm cell strainer, red blood cells were lysed with RBC lysis buffer (Solarbio, China). RPMI 1640 medium supplemented with MCSF (20 ng/mL, PEPROTECH, USA) and 10 % FBS was used to resuspend the cells before culture at a concentration of 2 ×

10^6 cells/mL. The medium was changed every two days, and M0 macrophages were obtained after seven days of culture. M0 macrophages were obtained and polarized for 48 h using RPMI 1640 medium containing 200 μg/mL soluble dECM alone (added 15 ng/mL IL-2) or Treg-conditioned medium mixed one-to-one with RPMI 1640 medium and supplemented with 200 μg/mL soluble dECM. Furthermore, M0 macrophages were polarized using the same conditions described above for 48 h in the presence of 100 ng/mL LPS (Sigma Aldrich, USA) and 20 ng/mL IFN-γ (PEPROTECH, USA). In addition, for M1 control, M0 macrophages were treated with 100 ng/mL LPS and 20 ng/mL IFN-γ for 48 h.

2.15. Western blotting

After macrophage polarization, the cells were lysed using RIPA buffer (Beyotime, China), mixed in proportion with loading buffer (Invitrogen, USA) and antioxidants (Invitrogen), and boiled for 10 min. The protein concentration was quantified using the BCA method (Thermo Fisher Scientific, USA). The samples were subsequently subjected to gel electrophoresis with preformed gels (10 %, Biovigen, China) at the same concentration in a Bio-Rad western blot electrophoresis system. After the proteins were transferred onto PVDF membranes (Merck Millipore, Germany), the membranes were blocked with skim milk. The membranes were incubated overnight with antibodies specific for the mannose receptor (1:1000, ab64693, Abcam, UK) and inducible nitric oxide synthase (iNOS) (1:1000, ab178945, Abcam, UK), followed by secondary antibodies conjugated to horseradish peroxidase (HRP, 1:20000, Abbkine, China). β-actin (1:10000, 66009, Proteintech, USA) was used as a loading control. The membranes were developed using an enhanced chemiluminescence method (Biosharp, China). The protein bands were visualized using a chemiluminescence imaging system (Tanon, China).

2.16. RNA extraction and real-time RT-PCR of mRNA

Total RNA was extracted using the TRIzol reagent (Invitrogen, USA) according to the manufacturer's protocol. Thereafter, 1000 ng of total RNA was reverse transcribed into cDNA using the PrimeScript RT reagent kit (TaKaRa, Japan). Real-time RT-PCR analysis was performed using Hieff qPCR SYBR Green Master Mix (YEASEN, China) and the qTOWER3G real-time RT-PCR System (Jena, Germany). The following cycling conditions were employed: 95 °C for 5 min, 40 cycles of 95 °C for 10 s, and 60 °C for 30 s. β-actin was used as the internal control for quantitation of the target mRNA. The primer sequences used for real-time RT-PCR are listed in Table S1.

2.17. Statistical analysis

The results were analyzed using GraphPad Prism software (version 9.0, USA). All results represent at least three independent experiments. All numerical values are expressed as mean ± SD. For comparisons between two experimental groups, the Student's t-test with a two-tailed distribution was performed. For multiple group comparisons, one-way analysis of variance (ANOVA) was performed using Tukey's post hoc test. All *P*-values ≤0.05 were considered to indicate statistical significance; the following asterisks are used to indicate the level of significance: *p ≤ 0.05, **p ≤ 0.01, ***p ≤ 0.001, ****p ≤ 0.0001. *P*-values >0.05 were considered to indicate no statistical significance (specified as "ns").

3. Results

3.1. Preparation and characterization of the dECM material

After obtaining fresh adult bovine native aortas, we used the SDS + CHAPS double detergent method for decellularization and obtained dECM. The efficiency of decellularization was evaluated using several strategies. HE staining of freshly harvested native aortas revealed dense structures (Fig. 1A). After decellularization, HE staining revealed no remaining cells (Fig. 1A), indicating complete removal of cells. SEM analysis of the dECM material revealed a 3D fiber network and confirmed the efficient removal of cellular components (Fig. 1B). We evaluated the preservation of collagen and elastic fibers in the dECM material via Masson and EVG staining (Fig. 1B). According to the results, ECM components, such as collagen and elastic fibers, were well preserved. Sirius red staining confirmed the presence of collagen fibers (Fig. S1 A). Overall, the histological examination revealed intact dECM structures, ideal matrix geometry, and no remaining cellular structures. Qualitative analysis via gel electrophoresis revealed that the DNA band was intact in the native group. Decellularization resulted in the substantial removal of this band. Furthermore, the residual DNA fragments almost disappeared (Fig. 1C). Electrophoretic analysis confirmed that dECM effectively lost DNA fragments. DNA content analysis corroborated the histological results, indicating that the dECM group contained less than 50 ng/mg dsDNA compared with the native group (Fig. 1D). According to the research community, a tissue must fulfill the following criteria to be characterized as "decellularized": (1) HE staining should reveal a complete absence of nuclear material in the dECM; (2) the length of the DNA fragment should be < 200 bp; and (3) the amount of double-stranded DNA should not exceed 50 ng/mg of the dECM's dry weight. In summary, we prepared decellularized materials that met current decellularization standards [39].

We tested whether the dECM contained residual decellularized detergent and determined its toxicity. *In vitro*, dECM was directly incubated with human fibroblasts for 48 h and fibroblast viability was analyzed using Taban Blue staining. Based on our observations, the dECM had no significant effect on cell viability (Fig. 1E). The CCK-8 assay revealed that different proportions of the dECM extract solution had no adverse effects on the viability of human fibroblasts compared with the control culture medium. Moreover, no toxicity of residual SDS was detected (Fig. 1F). A live/dead assay was used to assess cell viability. Human fibroblasts cultured in the extract medium were comparably viable to those cultured in control medium (Fig. 1G and H). Phalloidin staining revealed that the extract had no significant effect on the cytoskeleton (Fig. 1I and J). These results indicate the satisfactory biocompatibility of the dECM material. In terms of mechanical properties, the stress-strain curves were similar between the native material and dECM groups (Fig. S1 B); however, the Young's modulus was slightly reduced in the dECM group (Fig. S1 C). In addition, the ultimate tensile strength and ultimate tensile strain were slightly decreased in the dECM group, but were not statistically significant (Fig. S1 D, E). The suture retention strength was not significantly altered (Fig. S1 F). Therefore, decellularization treatment did not markedly damage the mechanical properties of the material. The results of the water contact angle test indicate that both the dECM and native materials were hydrophilic, with the dECM group being more hydrophilic than the native group (Fig. S1 G).

3.2. Tregs are recruited after dECM material implantation

We established a traumatic wound model in the mouse quadriceps femoris muscle and implanted the dECM material to observe dECM remodeling. Previous studies have shown that this model recapitulates the responses of immune cells to different extracellular matrix biomaterials [13,40]. The same mice underwent dECM implantation in the right leg and surgery without implantation in the left leg (sham). Histological analysis of cell infiltration in the dECM was performed at 3, 7, 14, and 28 days post-explantation. Histological findings revealed gradual infiltration of cells (HE) with progressive degradation of collagen (Masson's trichrome) and elastic fibers (EVG) over time (Fig. 2A). Sirius red staining also revealed gradual degradation of collagen fibers (Fig. S2 A). An early cellular response was observed three days after implantation, with cells limited to the implant edges. On day

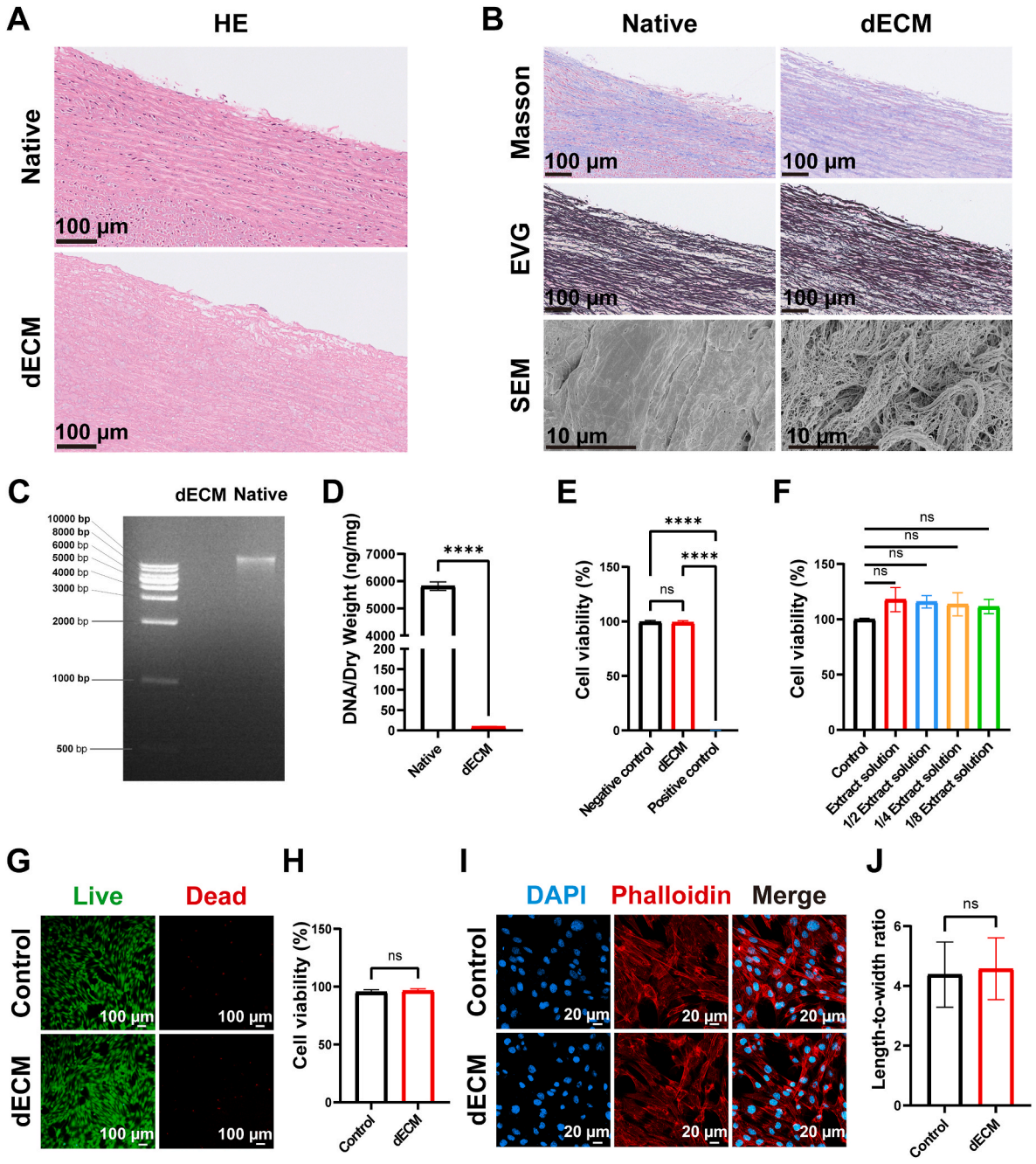

Fig. 1. Characterization of the dECM material. (A) HE staining images of the native and dECM materials. (B) Masson and EVG staining images, and SEM images of the native and dECM materials. (C) Gel electrophoresis depicts the size of DNA fragments remaining between the native and dECM materials. (D) PicoGreen for the DNA concentration between the native and dECM materials. (E) Direct contact cytotoxicity analysis. The viability of fibroblasts after contact with the dECM material was determined via trypan blue staining. Sterile gauze containing 10 % SDS (m/v) and plain sterile gauze were used as the positive and negative controls, respectively. (F–J) Extract contact cytotoxicity test. The viability of fibroblasts in contact with the dECM material extract was determined using a CCK-8 assay (F). (G) Representative images of fibroblasts stained with Calcein-AM (green) and PI (red). (H) Statistical analyses of viabilities according to the stain of Calcein-AM/PI. (I) Representative images of phalloidin staining and quantitative results of cell length-width ratio (J). Complete medium without dECM was placed under the same conditions during the extraction as a control group. ns = not significant, ****$p \leq 0.0001$. (For interpretation of the references to colour in this figure legend, the reader is referred to the Web version of this article.)

3, no capillaries, fibroblasts, or inflammatory cells were observed in the implant, and only few marginal fibroblasts, neutrophils, and monocytes infiltrated the edges of the dECM. Migration of cells from the host tissue to the dECM material was apparent at the dECM boundary and increased with prolonged implantation time. On day 7, numerous neutrophils, few monocytes, and fibroblasts infiltrated the implant edges. On day 14, an equal number of neutrophils infiltrated the edge of the implant, and multinuclear giant cells and fibroblast proliferation were observed. The marginal capillaries of the grafts were abundant and wrapped in a thick fibrous connective tissue. Fibroblast proliferation was observed in the middle of the implant; few neutrophils and capillaries were observed, and monocytes and multinucleated giant cells were rare. The intense cellular response at the graft edge subsided on days 7 and 14, indicating progressive cell migration and differentiation. On day 28, fibroblasts, neutrophils, and capillaries were observed on the implants. The implant was wrapped in thin fibrous connective tissue.

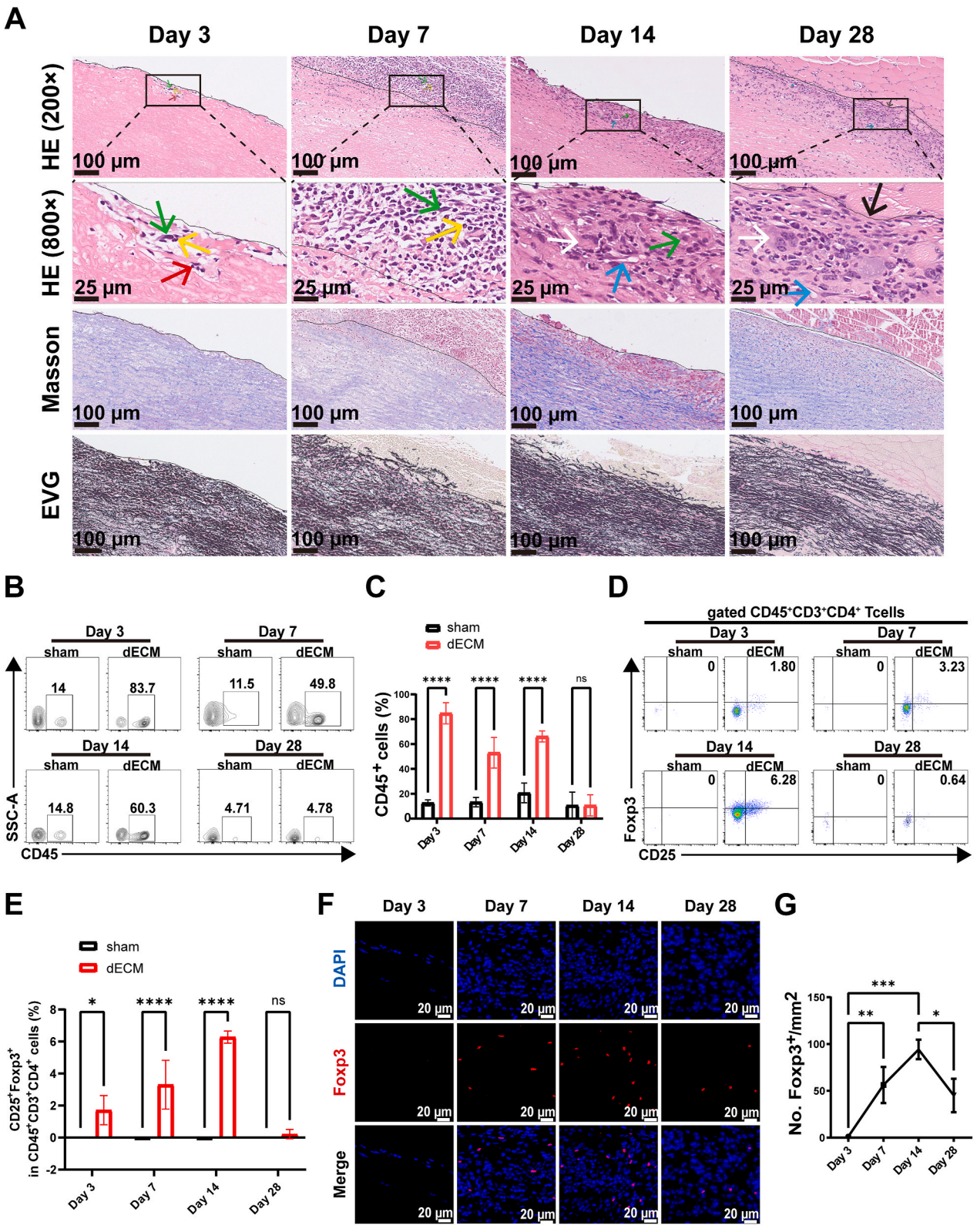

Fig. 2. Histological analysis and cell recruitment after implantation of the dECM material. (A) Representative images of dECM stained with HE, Masson, and EVG staining on days 3, 7, 14, and 28 after implantation in the mouse muscle traumatic model. Fibroblasts are indicated by green arrows, neutrophils by yellow arrows, monocytes by red arrows, capillaries by blue arrows, multinucleated giant cells by white arrows, and fibrous connective tissue by black arrows. The dECM boundaries are framed with black wire. (B, C) Representative FACS plots (B) and quantitative analysis (C) of the proportion of $CD45^+$ cells between the dECM and sham groups on days 3, 7, 14, and 28 after implantation. (D, E) Proportion of Tregs in the dECM and sham groups was determined on days 3, 7, 14, and 28 after implantation via flow cytometry (D) and quantitative analysis (E). (F, G) Representative images (F) and statistical plots (G) of $Foxp3^+$ cells in the dECM material, detected via immunofluorescence on days 3, 7, 14, and 28 after implantation. ns = not significant, *$p \leq 0.05$, **$p \leq 0.01$, ***$p \leq 0.001$, ****$p \leq 0.0001$. (For interpretation of the references to color in this figure legend, the reader is referred to the Web version of this article.)

Considering the important role of inflammation in graft remodeling [41], we used flow cytometry to detect the expression of $CD45^+$ leukocytes in the dECM and sham groups. As expected, the implantation of the dECM material significantly increased the recruitment of immune cells. Our data indicated that between days 3 and 14, the presence of the dECM material increased the proportion of $CD45^+$ cells at the implant site compared with that in the sham group (Fig. 2B and C). To monitor the presence of Tregs after implantation of the dECM material, we first used flow cytometry to analyze the temporal dynamics of Treg recruitment. $CD45^+$ cells were gated to obtain leukocytes. The $CD3^+CD4^+$ cell population was further gated from leukocytes to $CD4^+$ T-lymphocytes. The $CD25^+Foxp3^+$ population of $CD4^+$ T cells was considered Tregs (Fig. S2 B). Compared to the sham group, Tregs began to increase three days after implantation of the dECM material, continued to increase on day 7, and reached a peak expression on day 14 before gradually decreasing in the remodeling group (Fig. 2D and E). We also evaluated Treg infiltration into the dECM material. Immunofluorescence analysis of the dECM sections was performed at different time points after dECM implantation (Fig. 2F). The number of infiltrated Tregs was low on day 3 after implantation, increased significantly on day 7, peaked on day 14, and continued to increase until day 28 (Fig. 2G).

In summary, Tregs were demonstrated to be recruited after the implantation of the dECM material, and then infiltrated the material. The number of Tregs peaked at day 14 after implantation of the dECM material. Thus, this time point was selected to further analyze the contribution of Tregs to dECM material remodeling.

3.3. Reduced recruitment of Tregs leads to the rapid degradation of collagen and elastic fibers in the dECM material

As Tregs are recruited by dECM material, we reduced the number of Tregs by injecting PC61 anti-CD25 monoclonal antibody to determine the effect of Tregs on dECM remodeling. This antibody was used as it has been found to deplete Tregs *in vivo* and is widely used to study the biology of Tregs [27,42,43]. The mouse model was established via an intraperitoneal injection of a PC61 anti-CD25 monoclonal antibody or an isotype control antibody (IgG) on the first day before implantation, and supplemental injection of the antibody on day 7 (Fig. 3A). The study ended 14 days after implantation. The presence of Tregs in the peripheral blood of mice was randomly detected via flow cytometry from the day of dECM material implantation (day 0) to the end of the study (day 14) to ensure that Treg presence remained low throughout the study period (Fig. 3B, Fig. S3 A). On the last day of the study period, Tregs in the peripheral blood, lymph nodes, and dECM of mice were detected using flow cytometry, and a low number of Tregs was confirmed (Fig. 3C and D). In addition, Foxp3 immunofluorescence was performed on dECM sections. These results indicate that the number of Tregs infiltrating the dECM was significantly lower in the anti-CD25 group than in the control group (Fig. 3E and F).

To evaluate the contribution of Tregs to the remodeling response after dECM material implantation, we compared the histological section responses of the anti-CD25 group with those of the control group. HE staining revealed that the number and depth of the infiltrated cells at the edge of the dECM material in the anti-CD25 group were significantly higher than those in the control group (Fig. 3G). Neutrophils, capillaries, and fibroblasts were observed in both the graft groups (Fig. 3G). Immunofluorescence staining of the dECM sections revealed that the macrophage marker F4/80 was expressed in cells with several infiltrated edges in the anti-CD25 group (Fig. 3H). Masson's trichrome and EVG staining revealed that the collagen and elastic fibers of the dECM material in the anti-CD25 group were significantly fractured compared to those in the control group (Fig. 3I). The areas positive for collagen (Fig. 3J) and elastic (Fig. 3K) fibers in the dECM material also decreased significantly in the anti-CD25 group. Under a polarized light microscope, Sirius red staining revealed the breakage of collagen fibers and reduced the positive area of collagen fibers (Fig. S3 B). After removing the dECM, its collagen and elastin contents were determined using hydroxyproline and elastin detection kits. The collagen and elastin contents of the anti-CD25 group were also found to decrease (Fig. 3L,M).

Based on the above results, we observed significant damage and degradation of the dECM material in the anti-CD25 group. Premature degradation results in an early loss of structural integrity and an increased risk of rupture. The mechanical properties required to maintain the structure and function of the dECM material and the matrix required for the host cells to grow within the dECM material are insufficient. Remodeling failure occurs when the degradation rate of the dECM scaffold material exceeds the growth rate of the graft tissue [44].

3.4. Presence of anti-inflammatory and pro-regenerative phenotype of macrophages is trailing the decrease in Treg recruitment

As numerous macrophages were observed at the edge of the dECM material in the anti-CD25 group, we speculated that this occurrence may be an important cause of rapid degradation of the dECM material. Owing to the ability of Tregs to regulate inflammatory responses, we evaluated macrophage polarization in the control and anti-CD25 groups. Polarization of the dECM material-associated macrophages was assessed by measuring the expression of CD86 and CD206, which are markers of classically activated (M1) and alternately activated (M2) macrophages, respectively (Fig. S4). First, we evaluated the macrophage phenotypes of the cells infiltrating the dECM material using immunofluorescence staining (Fig. 4A). Detailed macrophage analysis revealed that most of the infiltrating dECM cells expressed F4/80 after implantation. The number of macrophages ($F4/80^+$ cells) in the dECM material was higher in the anti-CD25 group than in the control group (Fig. 4B). Moreover, the number of M2 macrophages in the reduced Treg expression group (anti-CD25 group) was significantly reduced to approximately half of that in the control group (Fig. 4C). Decreased Treg numbers had no significant effect on the proportion of M1 macrophages (Fig. 4D and E). We used flow cytometry to analyze the macrophage phenotype and obtained similar results (Fig. 4F). Reduced expression of Tregs can lead to impaired M2 polarization of macrophages in the dECM material and nearby tissues. The proportion of M2 macrophages ($CD45^+F4/80^+CD11b^+CD86^-CD206^+$) was reduced by approximately half in the anti-CD25 group compared to that in the control group (Fig. 4G). Simultaneously, the proportion of M1 ($CD45^+F4/80^+CD11b^+CD206^-CD86^+$) macrophages was not found to significantly differ between the anti-CD25 and control groups (Fig. 4H).

Constructive remodeling of the dECM has been reported to correlate with the M2 macrophage phenotypes [11]. When Treg recruitment decreased, the number of M2 macrophages in the immune microenvironment formed by the dECM material was significantly reduced, which negatively correlated with constructive remodeling of the dECM material.

3.5. Injection of the CD28-SA antibody promotes the increased recruitment of Tregs

Constructive remodeling is adversely affected by the rapid degradation of collagen and elastic fibers in the dECM material due to the reduced recruitment of Tregs. We focused on Treg expansion to enhance the constructive remodeling of the dECM material *in vivo*. CD28-SA antibody was used for Treg expansion. This antibody has been used in several studies for Treg expansion *in vivo* to investigate the functional role of Tregs [27,45,46]. The specific experimental protocol involved the intraperitoneal injection of the CD28-SA antibody the day before dECM implantation. The CD28-SA antibody was injected once on day 7 after implantation, and samples were collected on day 14 for testing (Fig. 5A). During the subsequent 14-day experimental period, Tregs were randomly detected in the peripheral blood of CD28-SA and control mice to confirm that the proportion of Tregs remained high during the experimental period (Fig. S5). The proportion of Tregs in the CD28-SA

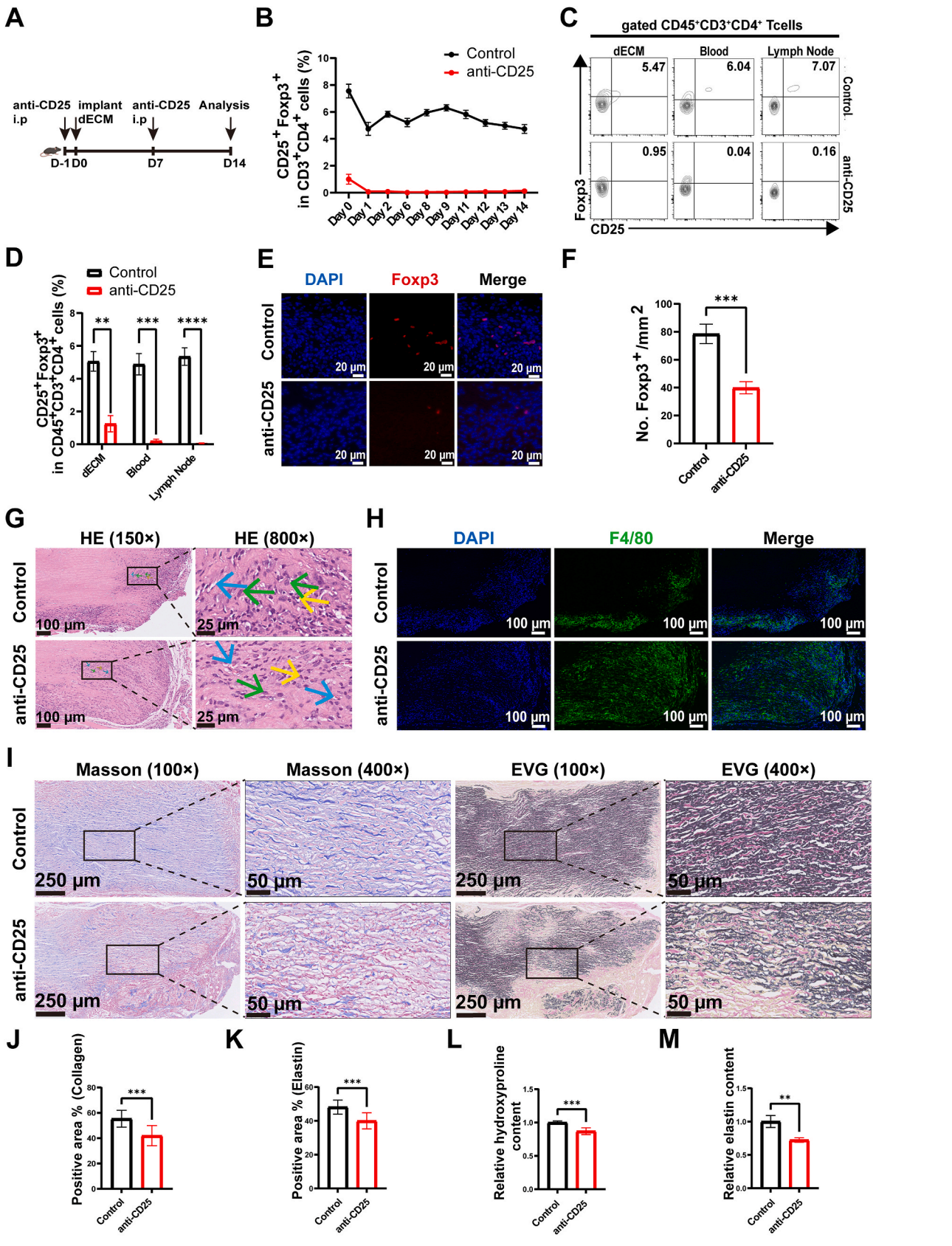

(caption on next page)

Fig. 3. Establishment of a mouse model with reduced Treg recruitment and histological analysis of the dECM material after implantation. (A) Schematic of the protocol for establishing a mouse model with reduced Treg recruitment. (B) Flow cytometry analysis of the proportion of Tregs in the peripheral blood of mice throughout the experimental period, indicating that the proportion of Tregs remains low. (C, D) Flow cytometry analysis results of the Treg proportions in the dECM, peripheral blood, and lymph nodes on day 14 after dECM material implantation, indicating a decrease in the proportion of Tregs. (E, F) Immunofluorescence images of $Foxp3^+$ cells from dECM material on day 14 after implantation show statistically decreased infiltration of Tregs into the dECM. (G) HE images of the dECM material in the anti-CD25 and control groups. Neutrophils are indicated by yellow arrows, capillaries by blue arrows, and fibroblasts by green arrows. (H) Immunofluorescence images of $F4/80^+$ cells of the dECM material between the anti-CD25 and control groups. (I) Representative images of Masson and EVG of the dECM material between the anti-CD25 and control groups. (J) Statistical analysis of the collagen fiber area percentage in the Masson images. (K) Statistical analysis of the elastic fiber area percentage in EVG images. (L) Hydroxyproline was used to determine the relative collagen content of the dECM material between the anti-CD25 and control groups. (M) Relative elastin content of the dECM material between the anti-CD25 and control groups. $^{**}p \leq 0.01$, $^{***}p \leq 0.001$, $^{****}p \leq 0.0001$. (For interpretation of the references to colour in this figure legend, the reader is referred to the Web version of this article.)

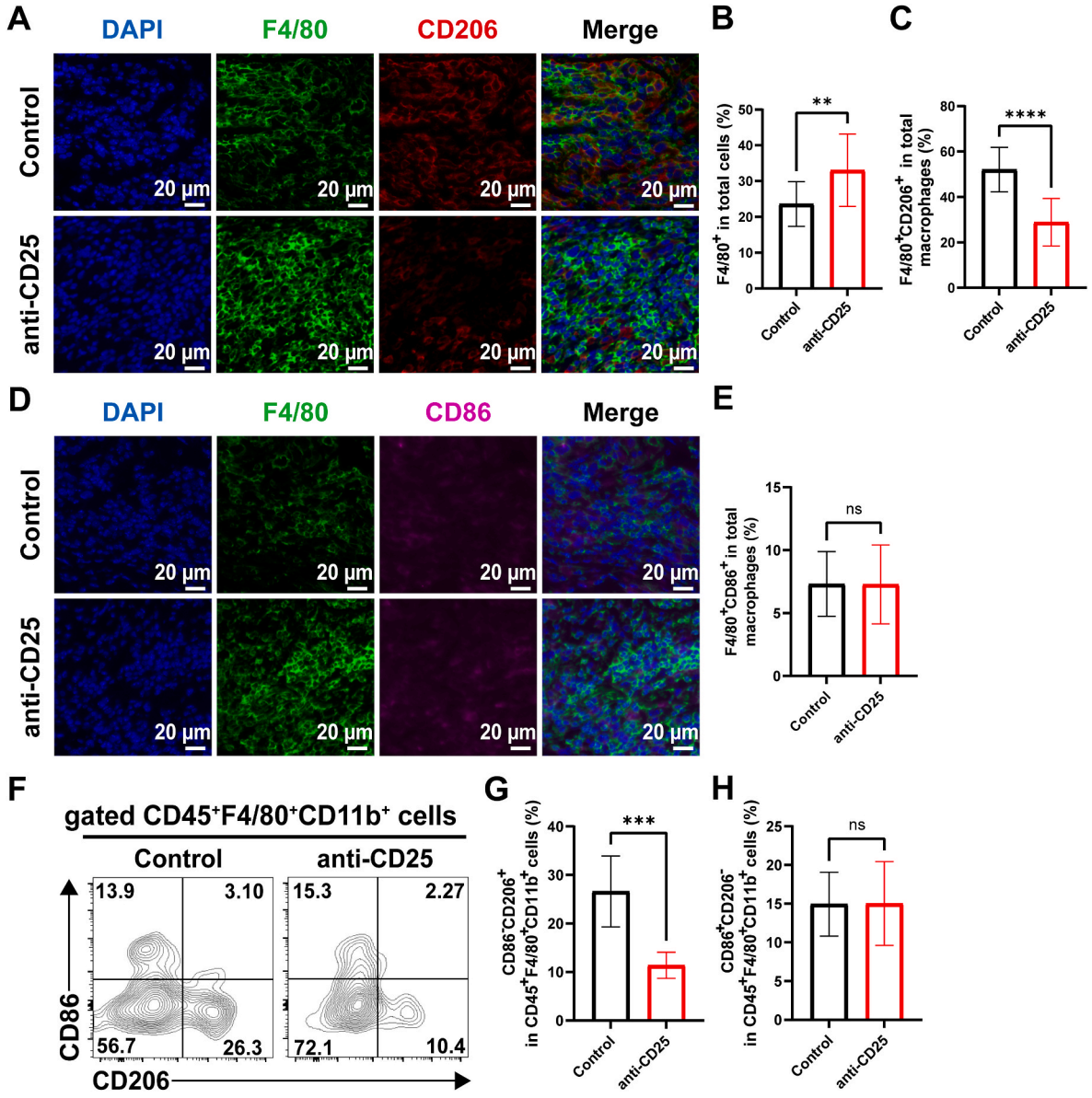

Fig. 4. Following a decrease in Treg recruitment, the presence of M2 macrophages decreases. (A–C) Representative immunofluorescence images (A), and quantitative analysis of total macrophages (B) and M2 macrophages (C). (D, E) Representative immunofluorescence images (D) and quantitative analysis (E) of M1 macrophages. (F) Representative FACS plots of macrophage polarization determined via flow cytometry. (G–H) Quantitative analysis of the proportion of M2 (G) and M1 (H) macrophages detected via flow cytometry. ns = significant, $^{**}p \leq 0.01$, $^{***}p \leq 0.001$, $^{****}p \leq 0.0001$.

group was normalized to that in the control group (Fig. 5B). On the first day after the administration of CD28-SA, the number of Tregs in the blood of mice increased more than threefold. During the subsequent experimental period, the number of Tregs in the CD28-SA group was approximately 2-fold higher than that in the control group (Fig. 5B). On day 14 after implantation of the dECM material, peripheral blood, lymph nodes, and dECM were collected from CD28-SA and control mice. The proportion of Tregs was determined using flow cytometry (Fig. 5C). The proportion of Tregs in the CD28-SA group was higher than that in the control group (Fig. 5D). Immunofluorescence was used to determine

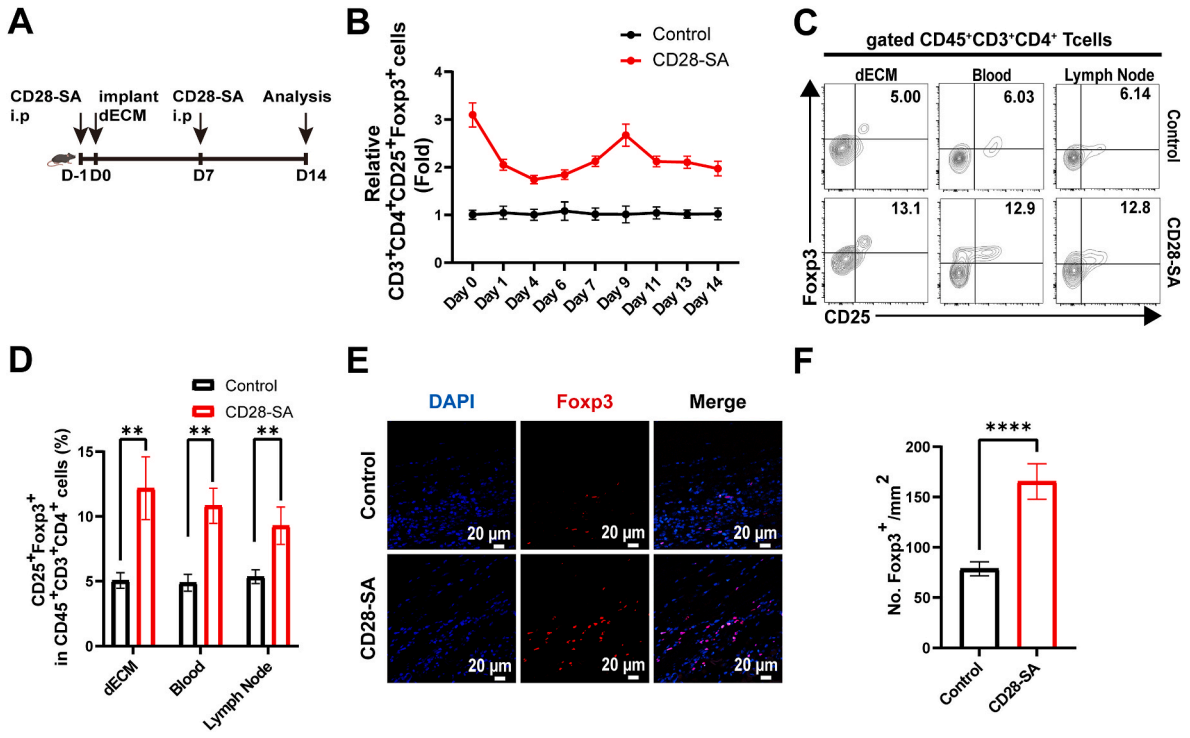

Fig. 5. Treg recruitment increases after injection of a CD28-SA antibody. (A) Schematic of the protocol for establishing a mouse model with increased Treg recruitment. (B) Flow cytometry results of the Treg proportion in the peripheral blood of mice indicate a persistently high proportion of Tregs throughout the study period, relative to the control group. The results were normalized relative to those of the control group. (C, D) Representative FACS plots of Treg proportion in dECM, peripheral blood, and lymph nodes on day 14 after dECM material implantation (C), with the accompanying statistical graph (D) indicating an increase in Treg proportion. (E, F) Immunofluorescence image of $Foxp3^+$ cells in dECM material on day 14 after implantation (E), with the accompanying statistical results (F) indicating an increase in Tregs infiltrating the dECM interior. **$p \leq 0.01$, ****$p \leq 0.0001$.

the presence of Tregs in the dECM material (Fig. 5E). Immunofluorescence staining for Foxp3 confirmed a significant increase in the recruitment of Tregs in the CD28-SA group (Fig. 5F).

3.6. Increased Treg recruitment promotes constructive remodeling of dECM material in vivo

To investigate changes in the dECM following increased Treg recruitment at the histological level, we used the HE, Masson, Sirius red, and EVG methods to stain the dECM. The CD28-SA group exhibited an improved remodeling effect compared with the control group. Histological analysis revealed that on day 14, host cell infiltration in the control group was concentrated around the dECM material (Fig. 6A). The control group exhibited a significant inflammatory response at the graft edge and dense inflammatory cells at the periphery of the dECM material. Large amounts of inflammatory cell infiltration, fibroblast proliferation, and capillaries were observed at graft margins (Fig. 6B). Little infiltration of host cells into the interior of the dECM material was observed and minimal infiltration of host cells into the scaffold was occasionally observed (Fig. 6C), whereas host cells in the CD28-SA group infiltrated the internal region of the dECM (Fig. 6D). The host remodeling response to the dECM material in the CD28-SA group was characterized by mild inflammatory responses at the edges of the dECM and homogeneous infiltration of host cells inside the dECM material (Fig. 6E). Histological sections revealed that several dECM materials contained fibrocytes. Even in the central region of certain dECM materials, inflammatory cells were almost absent and fibroblasts were gradually replaced by fibrocytes (Fig. 6F), indicating constructive remodeling. Neutrophils, monocytes, capillaries, and fibroblasts were also observed in the dECM material of the control group (Fig. 6G). The control dECM material was encapsulated in thicker fibrous connective tissue (Fig. 6H). Capillaries, monocytes, and other cells were observed in the dECM material in the CD28-SA group. Simultaneously, fibrocytes gradually replaced the fibroblasts (Fig. 6I). The dECM material in the CD28-SA group was encapsulated with thinner fibrous connective tissue than that in the control group (Fig. 6J).

The CD28-SA and control groups were scored using previously validated quantitative criteria for inflammatory and tissue remodeling responses on day 14 [11]. The evaluation criteria included cellular infiltration, multinucleated giant cells, vascularity, connective tissue organization, encapsulation, and degradation. Each evaluation criterion was scored on a scale of 0–3, with a higher score indicating a better constructive remodeling response and a lower score indicating a poorer remodeling response, such as a scar tissue or foreign body response. The CD28-SA group was found to have a higher histological score than the control group, suggesting that the increased recruitment of Tregs promoted constructive remodeling of the dECM material *in vivo* (Fig. 6K).

The dECM material rapidly degraded collagen and elastic fibers owing to reduced recruitment of Tregs (Fig. 3I). Therefore, after increasing Treg recruitment, the collagen and elastic fibers of the dECM material were examined using Masson, Sirius red, and EVG staining. Based on the staining results, the CD28-SA dECM maintained a consistent scaffold structure, providing sufficient matrix for the growth of host cells in the scaffold (Fig. 6L). By calculating the positive areas of collagen and elastic fibers, we found that the proportions of collagen (Fig. 6M) and elastic (Fig. 6N) fibers in the CD28-SA group were slightly higher than those in the control group; however, the difference was not statistically significant. In addition, the Sirius red staining results revealed no significant difference in the collagen fiber area (Fig. S6).

3.7. Increased Treg recruitment promotes the anti-inflammatory pro-regenerative phenotype of macrophages

As macrophages are key players in dECM material remodeling, we

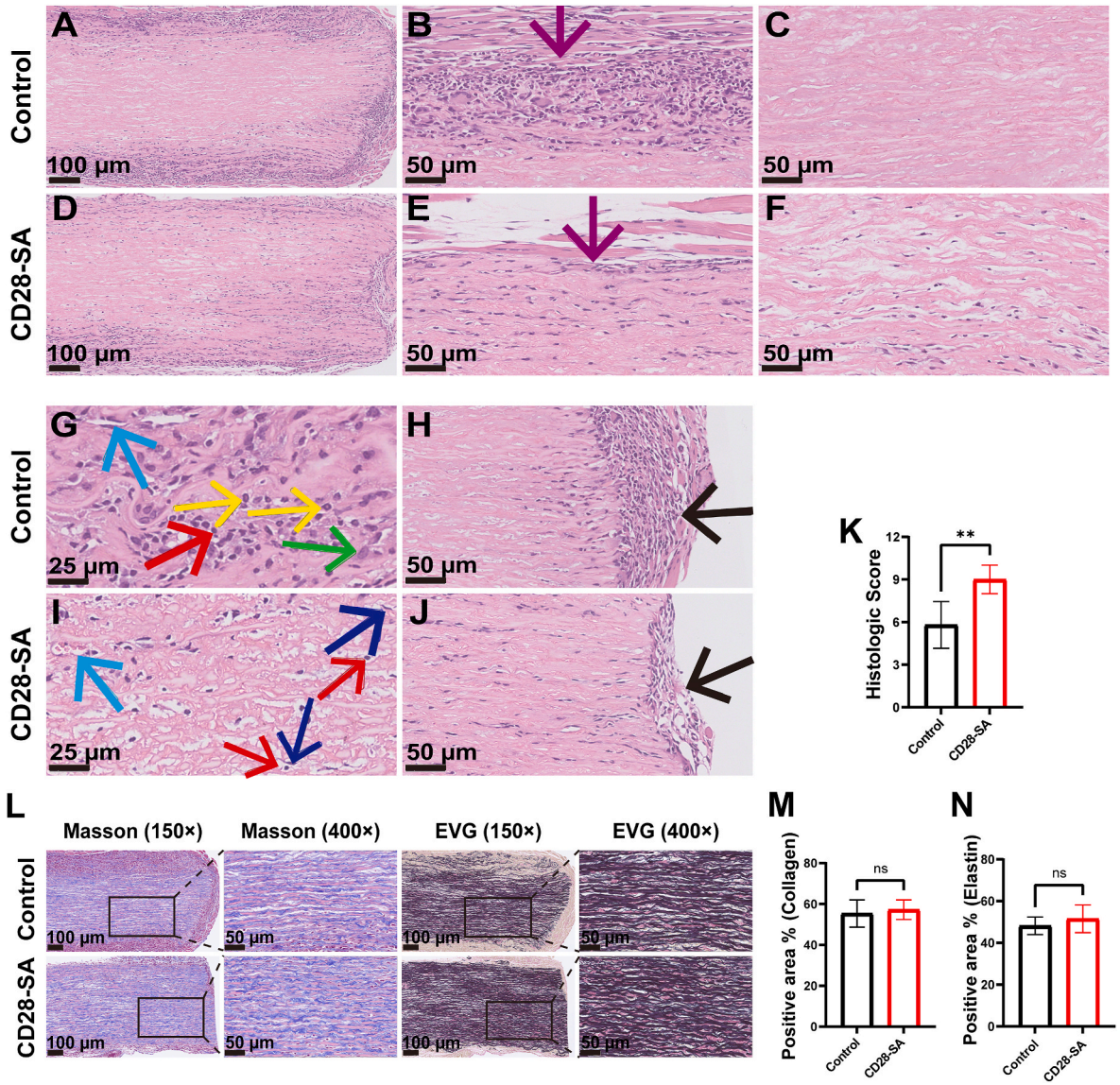

Fig. 6. Increased Treg recruitment promotes constructive remodeling of the dECM material *in vivo*. (A–J) Representative HE-stained images of the dECM material from the control and CD28-SA groups. Purple arrows indicate inflammatory cells at the edge of the dECM material. Neutrophils are indicated by yellow arrows, capillaries by blue arrows, fibroblasts by green arrows, monocytes by red arrows, and fibrous connective tissue by black arrows. The gradual replacement of fibroblasts (green arrows) by fibrocytes (dark blue arrows) in the CD28-SA group is shown. (K) Statistical graph of the histological quantitative scores for the inflammation and tissue remodeling responses, with the higher scores in the CD28-SA group implying an improved constructive remodeling response. (L) Representative Masson and EVG images of the dECM material. (M, N) Statistical plot for the percentage of collagen fiber area in Masson images (M) and the elastic fiber percentage area in EVG images (N). ns = not significant, **p ≤ 0.01. (For interpretation of the references to color in this figure legend, the reader is referred to the Web version of this article.)

focused on the recruitment of macrophages into the dECM. After observing that reduced Treg recruitment resulted in reduced polarization of M2 macrophages, we assessed the cell polarization status in the dECM material of mice in the CD28-SA group (Fig. 7A). Immunofluorescence detection of the dECM slices revealed that the dECM material of the CD28-SA group was infiltrated with fewer F4/80$^+$ macrophages than that of the control group (Fig. 7B). Interestingly, increased recruitment of Tregs promoted the polarization of macrophages toward the M2 phenotype (Fig. 7C) and suppressed polarization toward the M1 phenotype (Fig. 7D and E). Flow cytometry was used to detect macrophage polarization at the dECM and implant sites; similar results were obtained (Fig. 7F). M2 macrophages marked with CD206$^+$ displayed the opposite trend to that of M1 macrophages marked with CD86$^+$. Compared with the control group, the CD28-SA group had more M2 anti-inflammatory pro-regenerative macrophages (Fig. 7G) and a lower proportion of M1 pro-inflammatory macrophages (Fig. 7H).

To further detect the polarization status of macrophages, F4/80$^+$ macrophages were isolated from the dECM material, and transcriptome sequencing was subsequently performed. Compared with the control group, macrophages in the CD28-SA group upregulated the expression of 200 genes and downregulated those of 1323 genes, with the M2 macrophage marker CD163 being significantly overexpressed (Fig. 7I). Furthermore, we identified differentially expressed genes related to macrophage polarization and inflammatory responses (Fig. 7J). The expression levels of M2 macrophage-related *Mrc1* (also known as CD206), *CD163*, Arg*1,* and anti-inflammatory *IL4 and IL10* were significantly upregulated, whereas that of M1 macrophage-related *TNF* was significantly downregulated (Fig. 7J). In addition, in the CD28-SA group, the negative regulatory pro-inflammatory INF-γ and IL6 production signaling pathways of macrophages and M2-related VEGF

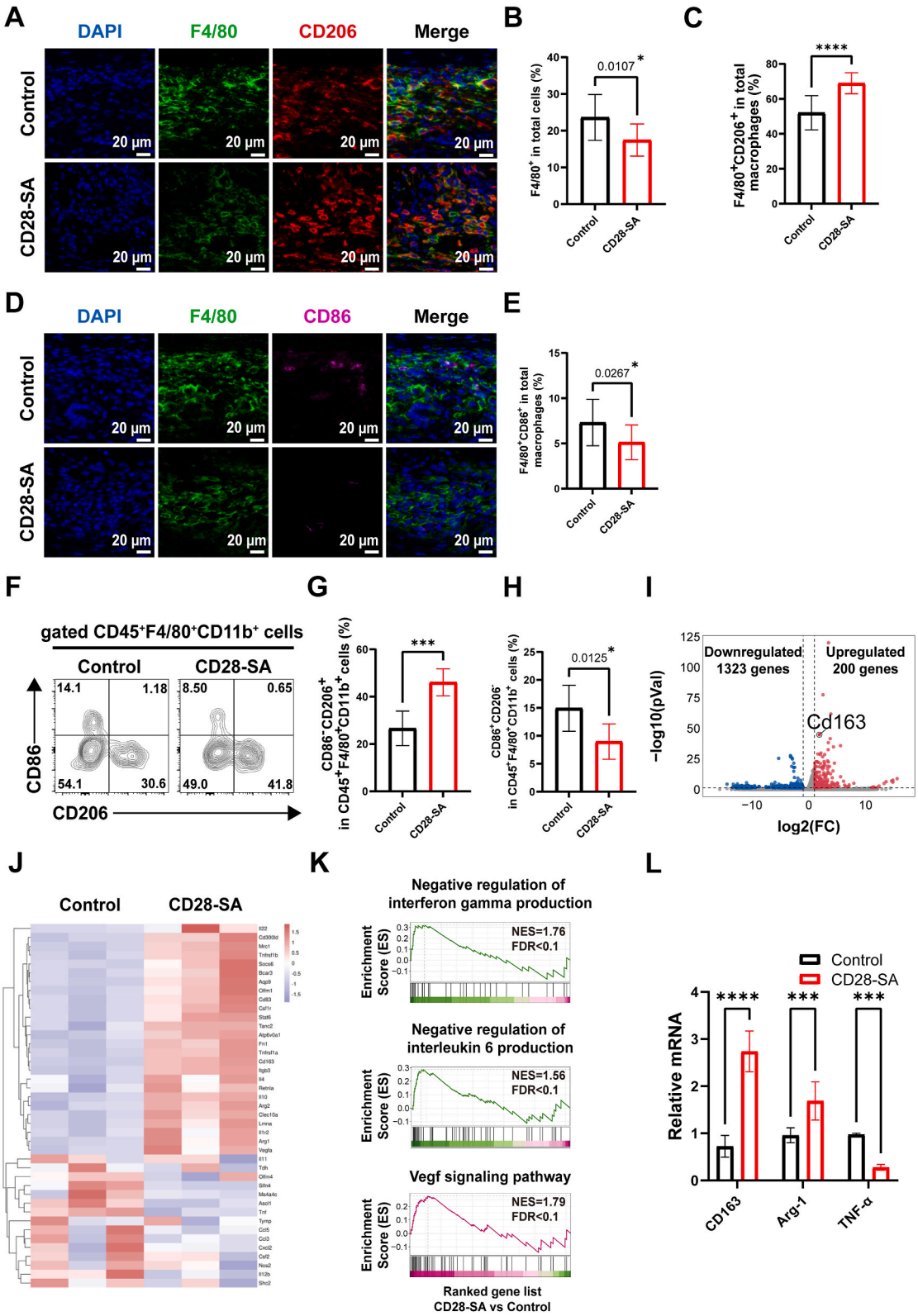

Fig. 7. Increased Treg recruitment promotes the anti-inflammatory and pro-regenerative phenotype of macrophages. (A–C) Representative immunofluorescence images (A), and quantitative analysis of total macrophages (B) and M2 macrophages (C). (D, E) Representative immunofluorescence images of M1 macrophages (D) and quantification analysis (E). The proportion of positive cells was counted by scanning and counting the entire dECM material. Statistical analysis was performed using T-test (n = 5) and the data are presented as mean ± SD. (F) Representative FACS plots of macrophage polarization. (G) Flow cytometry statistical analysis revealing an increased proportion of M2 macrophages. (H) Flow cytometry statistical analysis, depicting a reduction in the proportion of M1 macrophages. (I) Volcano plot of the differentially expressed genes in F4/80^{+} macrophages selected from the dECM material. (J) Heat map of macrophage polarization and inflammation-related gene expression (red: highly expressed; blue: low expression). (K) GSEA pathway enrichment map. (L) RT-qPCR results for verifying the expression of *CD163*, Arg*1*, and *TNF-α*. *p ≤ 0.05, ***p ≤ 0.001, ****p ≤ 0.0001. The test result of one asterisk (*) is annotated using the P-value on the graph. (For interpretation of the references to color in this figure legend, the reader is referred to the Web version of this article.)

signaling pathways were significantly upregulated (Fig. 7K). The same results were also obtained via qPCR verification, with the M2-associated *CD163* and Arg*1* being upregulated and M1-associated *TNF-α* being downregulated in macrophages of the CD28-SA group (Fig. 7L).

We found that an increase in Treg recruitment promoted constructive remodeling of the dECM material and was accompanied by an increase in M2 macrophages at the dECM and implant sites. On day 14, an increase in the number of M2 macrophages was associated with more positive remodeling outcomes [11]. Therefore, in the immune microenvironment formed by the dECM material, increased Treg recruitment promotes constructive remodeling of the dECM material by increasing the number of M2 macrophages.

3.8. Treg-conditioned medium promotes M2 macrophage polarization in vitro

In the immune microenvironment formed by the implantation of dECM material in mice, the proportion of M2 macrophages in the CD28-SA group increased (Fig. 7), whereas the proportion of M2 macrophages in the anti-CD25 group decreased (Fig. 4). We suggest that Tregs regulate the polarization of macrophages in the dECM material microenvironment and verified this experimentally *in vitro*.

First, we isolated and induced M0 macrophages (BMDMs) from mouse bone marrow. Using immunofluorescence, we determined that these cells exhibited the characteristic expression pattern of the macrophage surface marker CD68 (Fig. S7 A). After M0 macrophages were obtained, soluble dECM material was added to induce the polarization of M0 macrophages, and Treg-conditioned medium was added simultaneously. Macrophage phenotypes are influenced by the secreted cytokines of neighboring cells in the microenvironment. Accordingly, to determine whether Tregs influence macrophage polarization through secreted cytokines, we used Treg-conditioned medium. CD206 was defined as the M2 macrophage marker and CD86 was used as the M1 macrophage marker. Macrophage polarization was detected by flow cytometry using these markers (Fig. 8A). dECM was found to induce M0 macrophages to polarize toward M2 and the addition of Treg-conditioned medium significantly promoted M2 polarization (Fig. 8B). To further confirm the phenotype of differentiated macrophages, we performed western blot analysis to verify this phenomenon (Fig. 8C). The M2 macrophage marker CD206 protein further increased after the addition of the Treg-conditioned medium (Fig. 8D), whereas the M1-related iNOS protein was almost unexpressed. qRT-PCR revealed that the addition of Treg-conditioned medium significantly increased the expression of *CD206*, a phenotypic marker of M2 macrophages, compared to dECM alone. Meanwhile, the expression of the M2-related anti-inflammatory cytokine *IL10* was significantly upregulated (Fig. 8E). On the contrary, the addition of Treg-conditioned medium decreased the expression of *CD80*, a phenotypic marker of M1 macrophages, and that of the pro-inflammatory cytokine *TNF-α* (Fig. 8F). In addition, we induced M0 macrophage polarization with soluble dECM material in the presence of LPS and IFN-γ while adding Treg-conditioned medium. The addition of Treg-conditioned medium still significantly increased the expression of M2 macrophage-associated *CD206* and *Arg-1* in the presence of LPS and IFN-γ (Fig. S7 B). Moreover, this addition significantly inhibited the expression of M1 macrophage-associated *iNOS*, *IL-1β*, *TNF-α*, and *IL-6* (Fig. S7 C).

In summary, these results indicate that the dECM material directs the polarization of macrophages toward the M2 phenotype, while Treg-conditioned medium can increase the polarization toward M2 macrophages (even in the presence of LPS and IFN-γ), possibly due to the cytokines secreted by Tregs.

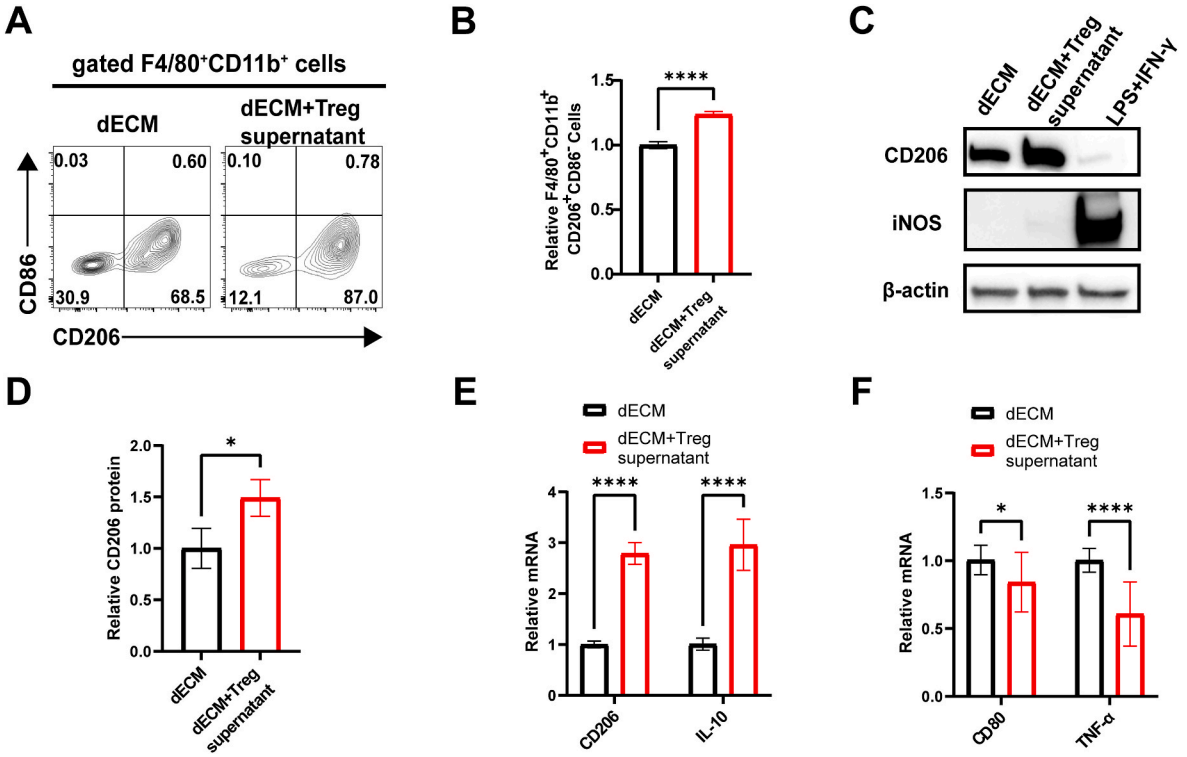

Fig. 8. Treg-conditioned medium promotes M2 macrophage polarization *in vitro*. (A, B) M0 BMDMs were polarized with soluble dECM material, while Treg-conditioned medium was added in parallel. Representative FACS plots of macrophage polarization using flow cytometry (A) and accompanying statistical analysis results (B). (C, D) Representative plots of CD206 and iNOS protein expression in macrophages based on Western blot (C), and corresponding quantitative analysis for CD206 protein expression (D). (E, F) Relative mRNA expression levels of M2 macrophage-associated *CD206* and *IL10* (E) and M1 macrophage-associated *CD80* and *TNF-α* (F) based on RT-qPCR. *p ≤ 0.05, ****p ≤ 0.0001.

4. Discussion

As critical components of the adaptive immune response, Tregs play an important role in inducing graft tolerance [47].In this study, we investigated the key role of Tregs in dECM remodeling. Increased recruitment of Tregs was found to promote the presence of M2 macrophages in the dECM material immune microenvironment and significantly enhance dECM remodeling.

Following implantation of the dECM material into mice, we detected Treg expression at the implant site. Over time, Treg expression increased, and Tregs infiltrated the dECM. On day 14, the number of Tregs in the microenvironment of the dECM material and inside the dECM peaked. Similar to our findings, the expression of Tregs was observed after implantation of ECM biomaterials [13]. As the immune system is the first responder to the implantation of biomaterials, we examined the expression of $CD45^+$ cells after implantation of dECM. The number of $CD45^+$ cells in the dECM material group was significantly higher than that in the sham-operated group without dECM material. This result implies that the dECM material-specific immune microenvironment develops in response to the implantation of the material rather than the surgical procedure. Similarly, biological and synthetic scaffolds induced a significantly elevated recruitment of immune cells compared with controls that did not receive implants, and the ECM scaffolds recruited the largest number of adaptive immune cells, mainly T cells [48].

The immune microenvironment of the dECM material can influence cell migration and tissue development within the biomaterial, gradually forming new viable tissues with potential persistence. Therefore, biomaterials must act as substrates to support appropriate host cell activity. To investigate whether Tregs are involved in the remodeling of the dECM material, we induced a decrease in the numbers of Tregs in mice using anti-CD25 monoclonal antibodies. Interestingly, after the recruitment of a reduced number of Tregs to the immune microenvironment and within the dECM material, the histological sections revealed that collagen and elastic fibers, the main components of the dECM material, were excessively fragmented and degraded 14 days after implantation. The hydroxyproline and elastin contents of the dECM material were detected, and the collagen and elastin contents of the anti-CD25 group were found to decrease. Moderate scaffold biomaterial degradation is necessary for tissue remodeling. However, the rapid and massive degradation in the early stages of implantation is not conducive to dECM material remodeling. During early implantation, the dECM material must remain intact in a three-dimensional manner to provide an adequate matrix for host cell ingrowth. As the half-life of vascular extracellular matrix collagen is in the order of months, to prevent long-term mechanical failure caused by collagen breakdown, numerous host cells that can maintain matrix integrity are required to remodel grafts [49]. Studies have shown that the SIS-ECM is completely degraded 10 weeks post-implantation [50,51]. For dermal ECM biomaterials, at least 50 % of the scaffold remains after 24 weeks of implantation [52].

Several cell infiltrates were found at the fracture sites of the dECM material collagen and elastic fibers in the anti-CD25 group. Host cells infiltrating the scaffold, such as neutrophils, macrophages, and lymphocytes, constantly secrete matrix metalloproteinases (MMPs) that catalyze the ECM components of the scaffold [53]. Immunofluorescence detection revealed that many cells infiltrating the dECM material in the anti-CD25 group expressed the macrophage marker F4/80. MMPs produced by macrophages target a wide variety of ECM components and aid matrix degradation [54]. Reactive oxygen species produced by macrophages can oxidize and degrade implant materials [55]. Macrophage ablation prevents the normal degradation of the ECM, suggesting a role for macrophages in ECM degradation [56]. Therefore, the large number of infiltrating macrophages may be related to the rapid degradation of the material, and the regulation of moderate levels of macrophage infiltration is essential for the function and regeneration of the material *in vivo*.

The macrophage phenotype has been implicated as a major determinant of the host response and clinical outcome of dECM materials [11,12,57]. We analyzed the microenvironment and internal macrophage phenotypes of the dECM material in the control and anti-CD25 groups. M2 macrophages in the dECM material were significantly decreased compared to those in the control; however, no significant change was found for the M1 macrophages. The ECM promotes the switch from M1 pro-inflammatory macrophages to M2 anti-inflammatory macrophages [58]. However, the mechanisms by which ECM scaffolds modulate the balance between the pro-inflammatory and anti-inflammatory phenotypes remain unclear. Studies have revealed that biological scaffolds derived from urinary bladder matrix tissue promote the M2 macrophage phenotype [11]. In this study, the dECM material favored the polarization of macrophages toward the M2 phenotype, which had a positive effect on remodeling. However, the recruitment of Tregs to the material microenvironment and inside the dECM decreased, and the presence of M2 pro-regenerative macrophages was significantly reduced. No significant changes in the number of M1 macrophages were observed, which might be due to the presence of dECM material in both the control and anti-CD25 groups, ultimately inducing macrophage polarization from M1 to M2. Macrophages are highly plastic and their phenotypes are determined by the tissue microenvironment. The epigenetic profile of tissue-resident macrophages is more dependent on the local tissue environment than on the cell lineage [59].

Stimulation with a CD28-specific monoclonal antibody (CD28-SA) induced the recruitment of Tregs, a further increase in M2 anti-inflammatory and pro-regenerative macrophages, and a decrease in M1 pro-inflammatory macrophages. Changes in Tregs in the immune microenvironment of dECM materials affected macrophage polarization. These results were confirmed by transcriptome sequencing of macrophages in the CD28-SA group. Macrophages in the CD28-SA group had a higher expression of *MRC1*, *CD163*, and Arg*1* than those in the control group. Co-culture of Tregs with monocytes induces macrophage polarization toward the M2 phenotype [30].To further examine the effects of the dECM material and Tregs on macrophage polarization, M0 bone marrow-derived macrophages were isolated and induced *in vitro*. Our findings indicated that the dECM material could induce M0 macrophages to polarize toward M2, and the addition of Treg-conditioned medium could further enhance polarization toward M2 (even in the presence of LPS and IFN-γ). Therefore, macrophage polarization promoted by Tregs may be related to cytokine secretion. The addition of Treg-conditioned medium further enhanced the expression of *IL10* in macrophages and inhibited the expression of the pro-inflammatory factor, *TNF-α*. Many investigators have developed strategies to promote M2 macrophage phenotypes and improve the clinical outcomes of dECM material [57]. Based on our current observations, the increased recruitment of Tregs can increase the number of M2 macrophages after dECM material implantation.

Increased recruitment of Tregs promotes constructive remodeling of dECM material *in vivo*. Unlike the large number of cells infiltrating the edge of the dECM material owing to decreased Treg expression, the high expression of Tregs increases the uniform infiltration of host cells into the dECM interior, which is beneficial for the next step of remodeling and regeneration. Moreover, the fibrous connective tissue enclosing the dECM material was thinner in the CD28-SA group than that in the control group, indicating decreased rejection. Porcine ECM scaffolds were not remodeled two years after implantation, suggesting limited infiltration of host cells, and scaffolds were not recellularized; only new tissue was formed around the original grafts [37]. Graft failure may occur when ECM scaffold degradation outpaces the growth of the perigraft tissue, which may result in graft failure [44]. We detected a significant increase in the M2 phenotype after increased recruitment of Tregs *in vivo*, which is known to be associated with structural remodeling. In addition, the presence of fibrocytes in the dECM material of the CD28-SA group suggested favorable constructive remodeling of the dECM material. After myocardial infarction, by increasing the number of

Tregs in the infarction zone, the polarization of M2 macrophages can be stimulated through soluble mediators, and the survival rate can be improved [27]. Based on our results, increased recruitment of Tregs can promote constructive remodeling of dECM material by increasing M2 macrophage polarization.

This study had several limitations. First, only macrophages with distinct M2 phenotype as $CD206^{+}$ $CD86^{-}$ or M1 $CD206^{-}$ $CD86^{+}$ were used for simplicity. This framework may oversimplify the macrophage heterogeneity *in vivo*. Indeed, the macrophage phenotype in the spectrum between the M1 and M2 extremes may be a co-expression of M1- and M2-type cells rather than a functional state with defined boundaries. Based on this macrophage variety, several *in vitro* guidelines have been proposed to distinguish between phenotypes [60]. Nonetheless, this approach has been useful as a predictor of *in vivo* ECM biomaterial remodeling outcomes [11]and a prognostic marker for certain diseases [61,62]. Second, the selection of a single time point limited our ability to assess the timing and magnitude of changes in Tregs that regulate macrophage polarization and participate in vascular dECM remodeling. After an increase in Treg recruitment, an increase in the elastic and collagen fibers of the dECM material was not obvious, which may be related to the selection of time points; prolonging the time may increase its significance. The mechanism of Treg recruitment after dECM implantation and the effects of dECM on cell behavior require further investigation. Meanwhile, the use of dECM scaffolds to achieve functional organ and tissues regeneration by regulating Treg participation deserves further investigation.

5. Conclusion

Overall, we used different approaches to determine the influence of Treg recruitment on dECM material remodeling. On one hand, with the recruitment of fewer Tregs, M2 macrophages decreased, and the collagen and elastic fibers in the dECM material were fractured and their content was decreased, which was not conducive to dECM material remodeling. In contrast, following increased recruitment of Tregs, the number of M2 macrophages increased, promoting constructive remodeling of the dECM material. *In vitro* experiments revealed that Tregs further enhanced the dECM material-induced M2 macrophage polarization through cytokine secretion. We observed a critical role of Tregs in the remodeling of dECM material. Therefore, the design of next-generation dECM materials and delivery of immunomodulators may be used to modulate Tregs to promote remodeling and regeneration. Our study offers new insights into the regulation of Tregs to enhance remodeling *in vivo* and provides new theoretical support for understanding the correlation between Tregs and dECM material remodeling.

CRediT authorship contribution statement

Hongjing Jiang: Writing – review & editing, Writing – original draft, Visualization, Methodology, Investigation, Formal analysis, Data curation, Conceptualization. **Xuheng Sun:** Methodology, Investigation. **Yindi Wu:** Methodology, Investigation. **Jianyi Xu:** Methodology. **Cong Xiao:** Methodology. **Qing Liu:** Investigation. **Lijun Fang:** Formal analysis. **Yuanfeng Liang:** Validation. **Jiahui Zhou:** Validation. **Yueheng Wu:** Supervision, Formal analysis. **Zhanyi Lin:** Writing – review & editing, Supervision, Resources, Project administration, Funding acquisition, Data curation, Conceptualization.

Declaration of competing interest

The authors declare that they have no known competing financial interests or personal relationships that could have appeared to influence the work reported in this paper.

Data availability

Data will be made available on request.

Acknowledgments

This work was supported by the Ji Hua Laboratory in Foshan City (X210111TD210) and the Open Project Fund of Guangdong Provincial People's Hospital (YKY-KF202208). The authors thank Jihua Laboratory for providing experimental equipment and space and the staff at Ji Hua's laboratory and Professor Guobing Chen of Jinan University for their assistance with this study. The graphical abstract was created with BioRender.com.

Appendix A. Supplementary data

Supplementary data to this article can be found online at https://doi.org/10.1016/j.mtbio.2024.101151.

References

[1] X. Zhang, X. Chen, H. Hong, R. Hu, J. Liu, C. Liu, Decellularized extracellular matrix scaffolds: recent trends and emerging strategies in tissue engineering, Bioact. Mater. 10 (2022) 15–31.
[2] L.E. Niklason, J.H. Lawson, Bioengineered human blood vessels, Science (New York, N.Y.) 370 (6513) (2020).
[3] R.J. Smith Jr., B. Nasiri, J. Kann, D. Yergeau, J.E. Bard, D.D. Swartz, S. T. Andreadis, Endothelialization of arterial vascular grafts by circulating monocytes, Nat. Commun. 11 (1) (2020) 1622.
[4] K.L. Spiller, R.R. Anfang, K.J. Spiller, J. Ng, K.R. Nakazawa, J.W. Daulton, G. Vunjak-Novakovic, The role of macrophage phenotype in vascularization of tissue engineering scaffolds, Biomaterials 35 (15) (2014) 4477–4488.
[5] L. Chung, D.R. Maestas Jr., F. Housseau, J.H. Elisseeff, Key players in the immune response to biomaterial scaffolds for regenerative medicine, Adv. Drug Deliv. Rev. 114 (2017) 184–192.
[6] D.P. Vasconcelos, A.P. Águas, M.A. Barbosa, P. Pelegrín, J.N. Barbosa, The inflammasome in host response to biomaterials: Bridging inflammation and tissue regeneration, Acta Biomater. 83 (2019) 1–12.
[7] M.T. Wolf, C.L. Dearth, C.A. Ranallo, S.T. LoPresti, L.E. Carey, K.A. Daly, B. N. Brown, S.F. Badylak, Macrophage polarization in response to ECM coated polypropylene mesh, Biomaterials 35 (25) (2014) 6838–6849.
[8] O. Veiseh, J.C. Doloff, M. Ma, A.J. Vegas, H.H. Tam, A.R. Bader, J. Li, E. Langan, J. Wyckoff, W.S. Loo, S. Jhunjhunwala, A. Chiu, S. Siebert, K. Tang, J. Hollister-Lock, S. Aresta-Dasilva, M. Bochenek, J. Mendoza-Elias, Y. Wang, M. Qi, D. M. Lavin, M. Chen, N. Dholakia, R. Thakrar, I. Lacík, G.C. Weir, J. Oberholzer, D. L. Greiner, R. Langer, D.G. Anderson, Size- and shape-dependent foreign body immune response to materials implanted in rodents and non-human primates, Nat. Mater. 14 (6) (2015) 643–651.
[9] T. Hasegawa, C.J. Hall, P.S. Crosier, G. Abe, K. Kawakami, A. Kudo, A. Kawakami, Transient inflammatory response mediated by interleukin-1β is required for proper regeneration in zebrafish fin fold, Elife 6 (2017).
[10] N. Kyritsis, C. Kizil, S. Zocher, V. Kroehne, J. Kaslin, D. Freudenreich, A. Iltzsche, M. Brand, Acute inflammation initiates the regenerative response in the adult zebrafish brain, Science (New York, N.Y.) 338 (6112) (2012) 1353–1356.
[11] B.N. Brown, R. Londono, S. Tottey, L. Zhang, K.A. Kukla, M.T. Wolf, K.A. Daly, J. E. Reing, S.F. Badylak, Macrophage phenotype as a predictor of constructive remodeling following the implantation of biologically derived surgical mesh materials, Acta Biomater. 8 (3) (2012) 978–987.
[12] S.F. Badylak, J.E. Valentin, A.K. Ravindra, G.P. McCabe, A.M. Stewart-Akers, Macrophage phenotype as a determinant of biologic scaffold remodeling, Tissue engineering, Part A 14 (11) (2008) 1835–1842.
[13] K. Sadtler, K. Estrellas, B.W. Allen, M.T. Wolf, H. Fan, A.J. Tam, C.H. Patel, B. S. Luber, H. Wang, K.R. Wagner, J.D. Powell, F. Housseau, D.M. Pardoll, J. H. Elisseeff, Developing a pro-regenerative biomaterial scaffold microenvironment requires T helper 2 cells, Science (New York, N.Y.) 352 (6283) (2016) 366–370.
[14] S. Sakaguchi, T. Yamaguchi, T. Nomura, M. Ono, Regulatory T cells and immune tolerance, Cell 133 (5) (2008) 775–787.
[15] S.L. Dahl, A.P. Kypson, J.H. Lawson, J.L. Blum, J.T. Strader, Y. Li, R.J. Manson, W. E. Tente, L. DiBernardo, M.T. Hensley, R. Carter, T.P. Williams, H.L. Prichard, M. S. Dey, K.G. Begelman, L.E. Niklason, Readily available tissue-engineered vascular grafts, Sci. Transl. Med. 3 (68) (2011) 68ra9.
[16] J. Li, J. Tan, M.M. Martino, K.O. Lui, Regulatory T-cells: potential regulator of tissue repair and regeneration, Front. Immunol. 9 (2018) 585.
[17] T.J. Murphy, N. Ni Choileain, Y. Zang, J.A. Mannick, J.A. Lederer, CD4+CD25+ regulatory T cells control innate immune reactivity after injury, J. Immunol. 174 (5) (2005) 2957–2963.
[18] A. Nosbaum, N. Prevel, H.A. Truong, P. Mehta, M. Ettinger, T.C. Scharschmidt, N. H. Ali, M.L. Pauli, A.K. Abbas, M.D. Rosenblum, Cutting edge: regulatory T cells facilitate Cutaneous wound healing, J. Immunol. 196 (5) (2016) 2010–2014.

[19] Y. Liu, L. Wang, T. Kikuiri, K. Akiyama, C. Chen, X. Xu, R. Yang, W. Chen, S. Wang, S. Shi, Mesenchymal stem cell-based tissue regeneration is governed by recipient T lymphocytes via IFN-γ and TNF-α, Nature medicine 17 (12) (2011) 1594–1601.
[20] H. Lei, K. Schmidt-Bleek, A. Dienelt, P. Reinke, H.D. Volk, Regulatory T cell-mediated anti-inflammatory effects promote successful tissue repair in both indirect and direct manners, Front. Pharmacol. 6 (2015).
[21] J.R. Mock, B.T. Garibaldi, N.R. Aggarwal, J. Jenkins, N. Limjunyawong, B. D. Singer, E. Chau, R. Rabold, D.C. Files, V. Sidhaye, W. Mitzner, E.M. Wagner, L. S. King, F.R. D'Alessio, Foxp3+ regulatory T cells promote lung epithelial proliferation, Mucosal Immunol. 7 (6) (2014) 1440–1451.
[22] L.W. Lai, K.C. Yong, Y.H. Lien, Pharmacologic recruitment of regulatory T cells as a therapy for ischemic acute kidney injury, Kidney Int. 81 (10) (2012) 983–992.
[23] D. Burzyn, W. Kuswanto, D. Kolodin, J.L. Shadrach, M. Cerletti, Y. Jang, E. Sefik, T. G. Tan, A.J. Wagers, C. Benoist, D. Mathis, A special population of regulatory T cells potentiates muscle repair, Cell 155 (6) (2013) 1282–1295.
[24] X. Meng, J. Yang, M. Dong, K. Zhang, E. Tu, Q. Gao, W. Chen, C. Zhang, Y. Zhang, Regulatory T cells in cardiovascular diseases, Nat. Rev. Cardiol. 13 (3) (2016) 167–179.
[25] F. Carbone, A. Nencioni, F. Mach, N. Vuilleumier, F. Montecucco, Pathophysiological role of neutrophils in acute myocardial infarction, Thromb. Haemostasis 110 (3) (2013) 501–514.
[26] F.R. D'Alessio, K. Tsushima, N.R. Aggarwal, E.E. West, M.H. Willett, M.F. Britos, M. R. Pipeling, R.G. Brower, R.M. Tuder, J.F. McDyer, L.S. King, CD4+CD25+Foxp3+ Tregs resolve experimental lung injury in mice and are present in humans with acute lung injury, J. Clin. Invest. 119 (10) (2009) 2898–2913.
[27] J. Weirather, U.D. Hofmann, N. Beyersdorf, G.C. Ramos, B. Vogel, A. Frey, G. Ertl, T. Kerkau, S. Frantz, Foxp3+ CD4+ T cells improve healing after myocardial infarction by modulating monocyte/macrophage differentiation, Circ. Res. 115 (1) (2014) 55–67.
[28] Y. Dombrowski, T. O'Hagan, M. Dittmer, R. Penalva, S.R. Mayoral, P. Bankhead, S. Fleville, G. Eleftheriadis, C. Zhao, M. Naughton, R. Hassan, J. Moffat, J. Falconer, A. Boyd, P. Hamilton, I.V. Allen, A. Kissenpfennig, P.N. Moynagh, E. Evergren, B. Perbal, A.C. Williams, R.J. Ingram, J.R. Chan, R.J.M. Franklin, D. C. Fitzgerald, Regulatory T cells promote myelin regeneration in the central nervous system, Nat. Neurosci. 20 (5) (2017) 674–680.
[29] D.S. Shouval, A. Biswas, J.A. Goettel, K. McCann, E. Conaway, N.S. Redhu, I. D. Mascanfroni, Z. Al Adham, S. Lavoie, M. Ibourk, D.D. Nguyen, J.N. Samsom, J. C. Escher, R. Somech, B. Weiss, R. Beier, L.S. Conklin, C.L. Ebens, F.G. Santos, A. R. Ferreira, M. Sherlock, A.K. Bhan, W. Müller, J.R. Mora, F.J. Quintana, C. Klein, A.M. Muise, B.H. Horwitz, S.B. Snapper, Interleukin-10 receptor signaling in innate immune cells regulates mucosal immune tolerance and anti-inflammatory macrophage function, Immunity 40 (5) (2014) 706–719.
[30] M.M. Tiemessen, A.L. Jagger, H.G. Evans, M.J. van Herwijnen, S. John, L.S. Taams, CD4+CD25+Foxp3+ regulatory T cells induce alternative activation of human monocytes/macrophages, Proc. Natl. Acad. Sci. U.S.A. 104 (49) (2007) 19446–19451.
[31] S.M. Melief, E. Schrama, M.H. Brugman, M.M. Tiemessen, M.J. Hoogduijn, W. E. Fibbe, H. Roelofs, Multipotent stromal cells induce human regulatory T cells through a novel pathway involving skewing of monocytes toward anti-inflammatory macrophages, Stem cells (Dayton, Ohio) 31 (9) (2013) 1980–1991.
[32] M. Panduro, C. Benoist, D. Mathis, T(reg) cells limit IFN-γ production to control macrophage accrual and phenotype during skeletal muscle regeneration, in: Proceedings of the National Academy of Sciences of the United States of America, vol. 115, 2018, pp. E2585–e2593, 11.
[33] L.L. McIntyre, S.A. Greilach, S. Othy, I. Sears-Kraxberger, B. Wi, J. Ayala-Angulo, E. Vu, Q. Pham, J. Silva, K. Dang, F. Rezk, O. Steward, M.D. Cahalan, T.E. Lane, C. M. Walsh, Regulatory T cells promote remyelination in the murine experimental autoimmune encephalomyelitis model of multiple sclerosis following human neural stem cell transplant, Neurobiol. Dis. 140 (2020) 104868.
[34] A. Castiglioni, G. Corna, E. Rigamonti, V. Basso, M. Vezzoli, A. Monno, A. E. Almada, A. Mondino, A.J. Wagers, A.A. Manfredi, P. Rovere-Querini, FOXP3+ T cells recruited to sites of sterile skeletal muscle injury regulate the fate of Satellite cells and Guide effective tissue regeneration, PLoS One 10 (6) (2015) e0128094.
[35] N. Ali, B. Zirak, R.S. Rodriguez, M.L. Pauli, H.A. Truong, K. Lai, R. Ahn, K. Corbin, M.M. Lowe, T.C. Scharschmidt, K. Taravati, M.R. Tan, R.R. Ricardo-Gonzalez, A. Nosbaum, M. Bertolini, W. Liao, F.O. Nestle, R. Paus, G. Cotsarelis, A.K. Abbas, M.D. Rosenblum, Regulatory T cells in skin facilitate epithelial stem cell differentiation, Cell 169 (6) (2017) 1119–1129.e11.
[36] Z. Mosala Nezhad, P. Baldin, A. Poncelet, G. El Khoury, Calcific degeneration of CorMatrix 4 Years after bicuspidization of unicuspid aortic valve, Ann. Thorac. Surg. 104 (6) (2017) e431–e433.
[37] J.L. Cox, J.M. Hammel, S.J. Radio, Evaluation of cellular ingrowth within porcine extracellular matrix scaffolding in congenital heart disease surgery, Cardiovascular pathology : the official, journal of the Society for Cardiovascular Pathology 39 (2019) 54–60.
[38] J.L. Dziki, D.S. Wang, C. Pineda, B.M. Sicari, T. Rausch, S.F. Badylak, Solubilized extracellular matrix bioscaffolds derived from diverse source tissues differentially influence macrophage phenotype, Journal of biomedical materials research. Part A 105 (1) (2017) 138–147.
[39] P.M. Crapo, T.W. Gilbert, S.F. Badylak, An overview of tissue and whole organ decellularization processes, Biomaterials 32 (12) (2011) 3233–3243.
[40] K. Sadtler, S.D. Sommerfeld, M.T. Wolf, X. Wang, S. Majumdar, L. Chung, D. S. Kelkar, A. Pandey, J.H. Elisseeff, Proteomic composition and immunomodulatory properties of urinary bladder matrix scaffolds in homeostasis and injury, Semin. Immunol. 29 (2017) 14–23.
[41] J.D. Roh, R. Sawh-Martinez, M.P. Brennan, S.M. Jay, L. Devine, D.A. Rao, T. Yi, T. L. Mirensky, A. Nalbandian, B. Udelsman, N. Hibino, T. Shinoka, W.M. Saltzman, E. Snyder, T.R. Kyriakides, J.S. Pober, C.K. Breuer, Tissue-engineered vascular grafts transform into mature blood vessels via an inflammation-mediated process of vascular remodeling, in: Proceedings of the National Academy of Sciences of the United States of America, vol. 107, 2010, pp. 4669–4674, 10.
[42] Y.Y. Setiady, J.A. Coccia, P.U. Park, In vivo depletion of CD4+FOXP3+ Treg cells by the PC61 anti-CD25 monoclonal antibody is mediated by FcgammaRIII+ phagocytes, Eur. J. Immunol. 40 (3) (2010) 780–786.
[43] M. Sharma, M.P. Schlegel, M.S. Afonso, E.J. Brown, K. Rahman, A. Weinstock, B. E. Sansbury, E.M. Corr, C. van Solingen, G.J. Koelwyn, L.C. Shanley, L. Beckett, D. Peled, J.J. Lafaille, M. Spite, P. Loke, E.A. Fisher, K.J. Moore, Regulatory T cells License macrophage pro-resolving functions during atherosclerosis regression, Circ. Res. 127 (3) (2020) 335–353.
[44] K.M. Naegeli, M.H. Kural, Y. Li, J. Wang, E.A. Hugentobler, L.E. Niklason, Bioengineering human tissues and the future of vascular replacement, Circ. Res. 131 (1) (2022) 109–126.
[45] M.M. Zaiss, B. Frey, A. Hess, J. Zwerina, J. Luther, F. Nimmerjahn, K. Engelke, G. Kollias, T. Hünig, G. Schett, J.P. David, Regulatory T cells protect from local and systemic bone destruction in arthritis, J. Immunol. 184 (12) (2010) 7238–7246.
[46] D. Langenhorst, T. Gogishvili, E. Ribechini, S. Kneitz, K. McPherson, M.B. Lutz, T. Hünig, Sequential induction of effector function, tissue migration and cell death during polyclonal activation of mouse regulatory T-cells, PLoS One 7 (11) (2012) e50080.
[47] H. Waldmann, R. Hilbrands, D. Howie, S. Cobbold, Harnessing FOXP3+ regulatory T cells for transplantation tolerance, J. Clin. Invest. 124 (4) (2014) 1439–1445.
[48] K. Sadtler, M.T. Wolf, S. Ganguly, C.A. Moad, L. Chung, S. Majumdar, F. Housseau, D.M. Pardoll, J.H. Elisseeff, Divergent immune responses to synthetic and biological scaffolds, Biomaterials 192 (2019) 405–415.
[49] R.D. Kirkton, M. Santiago-Maysonet, J.H. Lawson, W.E. Tente, S.L.M. Dahl, L. E. Niklason, H.L. Prichard, Bioengineered human acellular vessels recellularize and evolve into living blood vessels after human implantation, Sci. Transl. Med. 11 (485) (2019).
[50] T.W. Gilbert, A.M. Stewart-Akers, A. Simmons-Byrd, S.F. Badylak, Degradation and remodeling of small intestinal submucosa in canine Achilles tendon repair, The Journal of bone and joint surgery. American 89 (3) (2007) 621–630.
[51] R.D. Record, D. Hillegonds, C. Simmons, R. Tullius, F.A. Rickey, D. Elmore, S. F. Badylak, In vivo degradation of 14C-labeled small intestinal submucosa (SIS) when used for urinary bladder repair, Biomaterials 22 (19) (2001) 2653–2659.
[52] L.E. Carey, C.L. Dearth, S.A. Johnson, R. Londono, C.J. Medberry, K.A. Daly, S. F. Badylak, In vivo degradation of 14C-labeled porcine dermis biologic scaffold, Biomaterials 35 (29) (2014) 8297–8304.
[53] A.B. Gardner, S.K. Lee, E.C. Woods, A.P. Acharya, Biomaterials-based modulation of the immune system, BioMed Res. Int. 2013 (2013) 732182.
[54] A. Page-McCaw, A.J. Ewald, Z. Werb, Matrix metalloproteinases and the regulation of tissue remodelling, Nat. Rev. Mol. Cell Biol. 8 (3) (2007) 221–233.
[55] T.B. Wissing, V. Bonito, E.E. van Haaften, M. van Doeselaar, M. Brugmans, H. M. Janssen, C.V.C. Bouten, A. Smits, Macrophage-driven biomaterial degradation depends on scaffold microarchitecture, Front. Bioeng. Biotechnol. 7 (2019) 87.
[56] J.E. Valentin, A.M. Stewart-Akers, T.W. Gilbert, S.F. Badylak, Macrophage participation in the degradation and remodeling of extracellular matrix scaffolds, Tissue engineering, Part A 15 (7) (2009) 1687–1694.
[57] B.N. Brown, B.D. Ratner, S.B. Goodman, S. Amar, S.F. Badylak, Macrophage polarization: an opportunity for improved outcomes in biomaterials and regenerative medicine, Biomaterials 33 (15) (2012) 3792–3802.
[58] I.T. Swinehart, S.F. Badylak, Extracellular matrix bioscaffolds in tissue remodeling and morphogenesis, Dev. Dynam. : an official publication of the American Association of Anatomists 245 (3) (2016) 351–360.
[59] Y. Lavin, D. Winter, R. Blecher-Gonen, E. David, H. Keren-Shaul, M. Merad, S. Jung, I. Amit, Tissue-resident macrophage enhancer landscapes are shaped by the local microenvironment, Cell 159 (6) (2014) 1312–1326.
[60] P.J. Murray, J.E. Allen, S.K. Biswas, E.A. Fisher, D.W. Gilroy, S. Goerdt, S. Gordon, J.A. Hamilton, L.B. Ivashkiv, T. Lawrence, M. Locati, A. Mantovani, F.O. Martinez, J.L. Mege, D.M. Mosser, G. Natoli, J.P. Saeij, J.L. Schultze, K.A. Shirey, A. Sica, J. Suttles, I. Udalova, J.A. van Ginderachter, S.N. Vogel, T.A. Wynn, Macrophage activation and polarization: nomenclature and experimental guidelines, Immunity 41 (1) (2014) 14–20.
[61] S. Nassiri, I. Zakeri, M.S. Weingarten, K.L. Spiller, Relative expression of proinflammatory and antiinflammatory genes reveals differences between healing and nonhealing human chronic diabetic foot ulcers, J. Invest. Dermatol. 135 (6) (2015) 1700–1703.
[62] P. Dong, L. Ma, L. Liu, G. Zhao, S. Zhang, L. Dong, R. Xue, S. Chen, CD86^{+}/CD206^{+}, diametrically polarized tumor-associated macrophages, predict hepatocellular carcinoma patient prognosis, Int. J. Mol. Sci. 17 (3) (2016) 320.